Computers and Fluids 000 (2016) 1–20

Contents lists available at ScienceDirect

Computers and Fluids

journal homepage: www.elsevier.com/locate/compfluid

The emergence of fast oscillations in a reduced primitive equation model and its implications for closure theories☆

Mickaël D. Chekroun[a,*], Honghu Liu[b], James C. McWilliams[a]

[a] Department of Atmospheric & Oceanic Sciences, University of California, Los Angeles, CA 90095-1565, USA
[b] Department of Mathematics, Virginia Polytechnic Institute and State University, Blacksburg, Virginia 24061, USA

ARTICLE INFO

Article history:
Received 15 May 2016
Accepted 5 July 2016
Available online xxx

MSC:
34F05
35R60
37L05
37L55
37L65
60H15

Keywords:
Parameterizing manifolds
Slow manifolds
Slow conditional expectations
Emergence of fast oscillations
Balance equations

ABSTRACT

The problem of emergence of fast gravity-wave oscillations in rotating, stratified flow is reconsidered. Fast inertia-gravity oscillations have long been considered an impediment to initialization of weather forecasts, and the concept of a "slow manifold" evolution, with no fast oscillations, has been hypothesized. It is shown on a reduced Primitive Equation model introduced by Lorenz in 1980 that fast oscillations are absent over a finite interval in Rossby number but they can develop brutally once a critical Rossby number is crossed, in contradistinction with fast oscillations emerging according to an exponential smallness scenario such as reported in previous studies, including some others by Lorenz. The consequences of this dynamical transition on the closure problem based on slow variables is also discussed. In that respect, a novel variational perspective on the closure problem exploiting manifolds is introduced. This framework allows for a unification of previous concepts such as the slow manifold or other concepts of "fuzzy" manifold. It allows furthermore for a rigorous identification of an optimal limiting object for the averaging of fast oscillations, namely the optimal parameterizing manifold (PM). It is shown through detailed numerical computations and rigorous error estimates that the manifold underlying the nonlinear Balance Equations provides a very good approximation of this optimal PM even somewhat beyond the emergence of fast and energetic oscillations.

1. Introduction

The concept of a "slow manifold" was presented in a didactic paper by Leith [37] in an attempt to filter out, on an analytical basis, the fast gravity waves for the initialization of the Primitive Equations (PE) of the atmosphere. The motivation was that small errors in a "proper balance" between the fast time-scale motion associated with gravity waves and slower motions such as associated with the Rossby waves, lead typically to an abnormal evolution of gravity waves, which in turn can cause appreciable deviations of weather forecasts. This filtering approach has a long history in forecast initialization, e.g. [3,43].

To provide a remedy to this initialization problem, Leith proposed that a "proper balance" between fast and slow motion may be postulated to exist, and, using the language of dynamical system theory, it was thought of as a manifold in the phase space of the PE consisting of orbits for which gravity waves motion is absent. An iteration scheme was then developed to find from the observed state in phase space a corresponding initial state on such a "slow" manifold, so that weather forecasts with these initial states can be accurate on the same time scales as those of Rossby waves. In Leith's treatment the filtering was equivalent to the Quasigeostrophic approximation for asymptotically small Rossby number, V/fL (V a typical horizontal velocity, f the Coriolis frequency, and L a horizontal length). Solutions to the Quasigeostrophic model remain slow for all time.

This idea was appealing for dealing with this filtering problem, but uncertainty in the definition of a slow manifold for finite Rossby number has led to a proliferation of different schemes, on one hand, and to the question of whether a precise definition can be provided at all on the other hand, i.e., whether a slow invariant manifold even exists at finite Rossby number.

The latter question is especially interesting from a theoretical point of view. Lorenz [41] was probably the first to address in at-

☆ This article is dedicated to Chuck, a longtime colleague of the 3rd author, and it is presented as fruitful conversations across our generations.

* Corresponding author.
E-mail addresses: mchekroun@atmos.ucla.edu (M.D. Chekroun), hhliu@vt.edu (H. Liu), jcm@atmos.ucla.edu (J.C. McWilliams).

http://dx.doi.org/10.1016/j.compfluid.2016.07.005

mospheric sciences the problem of definition and existence of a slow manifold as a dynamical system object, although the concept was analyzed by mathematicians prior to that work [20,21,56]. In that respect, he introduced a further simplified version of his truncated, nine-dimensional PE model derived originally in [40] to reduce it to a five dimensional system of ordinary differential equations (ODEs). He then identified the variables representing gravity waves as the ones which can exhibit fast oscillations, and defined the slow manifold as an invariant manifold in the five dimensional phase space for which fast oscillations never develop. In a subsequent work, Lorenz and Krishnamurthy [38] after introducing forcing and damping in the 5-variable model of [41], identified an orbit which by construction has to lie on the slow manifold. They followed its evolution numerically to show that sooner or later fast oscillations developed, thereby implying that a slow manifold according to their definition did not exist for the model.

By relying on quadratic integral of motions, it was shown in [4] that the 5-variable model of [41] reduces to the following slow-fast system of four equations:

$$\begin{aligned}\dot{\theta} &= w - \epsilon b y,\\ \dot{w} &= -\sin(\theta),\\ \epsilon\dot{x} &= -y,\\ \epsilon\dot{y} &= x + b\sin(\theta).\end{aligned} \tag{1.1}$$

In this form, the Lorenz–Krishnamurthy (LK) system (without dissipation and forcing terms) can be understood as describing the dynamics of a slow nonlinear pendulum (w, θ), with angle θ from the vertical, coupled in some way with a harmonic oscillator that can be thought as a stiff spring with constant ϵ^{-1} and of extension (x, y).

By a delicate usage of tools from the geometric singular perturbation theory [32] to "blow up" the region near the singularity (of a saddle-center type)[1] at the origin, it was rigorously shown in [4] that the time evolution of initial data lying on the (homoclinic) orbit considered in [38] will invariably develop fast oscillations in the course of time. This result provided a partial answer to the question raised in [38] about the existence of a slow manifold, at least in the conservative case.

Nevertheless, the outcome of such a study was seemingly in contradiction with those of [30], which show, by relying essentially on a local normal form analysis, that for the (dissipative) LK system, a slow manifold exists. As noted by Lorenz himself in [42], again what one means by "slow manifold" does matter. In [30], the existence of such a manifold was only local in the phase space, which did not exclude thus the emergence of fast oscillations as one leaves the neighborhood of the relevant portion of the phase space, here near the Hadley point $(0, F, 0, 0, 0)$.[2] Actually, the authors of [15] proved that a global manifold can be identified, but that this manifold is not void of fast oscillations and thus is not slow in the language of dynamical system theory.

The implications of the results of [15] combined with the original numerical results of [38], advocated thus an interesting physical mechanism for the spontaneous generation of inertia-gravity waves. Lorenz and Krishnamurthy used numerical solutions to show in the low-Rossby-number, Quasigeostrophic regime that the amplitude of the inertia-gravity waves that are generated is actually exponentially small, i.e. proportional to $\exp(-\alpha/\epsilon)$, where $\epsilon < <1$ is the relevant small parameter and $\alpha > 0$ is a structural constant. The generation of exponentially small inertia-gravity oscillations takes place for $t > 0$, whereas the solutions are well balanced for $t \to -\infty$.

By means of elegant exponential-asymptotic techniques, Vanneste in [59] provided an estimate for the amplitude of the fast inertia-gravity oscillations that are generated spontaneously, through what is known as of the crossing of Stokes lines as time evolves, i.e. the crossing of particular time instants corresponding to the real part of poles close to the real (time) axis, in the meromorphic extension of the solutions (in complex time). These analytic results showed thus an exponentially small "fuzziness" scenario (in Rossby number) to hold for the LK system; exponential smallness then has been argued to hold for more realistic flows by several complementary studies or experiments; e.g. [22,51,60,61,63,64].

Going back to the original reduced PE model of Lorenz [40], we show on a rescaled version (described in Section 2.2) that while the emergence of small-amplitude fast oscillations is still synonymous of the breakdown of (exact) slaving principles, a sharp dynamical transition occurs as a parameter ϵ, which can be identified with the Rossby number, crosses a critical value ϵ_*. Such a sudden transition was pointed out in [62]. We conduct in this work a more detailed examination of this transition with in particular smaller time steps and a higher-order time-stepping scheme than used in [62]. This transition corresponds to the emergence of fast gravity waves that can contain a significant fraction of the energy (up to $\sim 40\%$) as time evolves and that may either populate transient behaviors of various lengths or persist in an intermittent way as both time flows and ϵ varies beyond ϵ_*; see Section 2.3. Although the mathematical characterization of this transition is an interesting question *per se*, we focus in this article on the consequences of such a critical transition on the closure problem for the slow rotational variables. For that purpose we revisit the Balance Equations (BE) [27] within the framework of *parametrizing manifolds (PMs)* introduced in [9,12] for different but related parameterization objectives.

As shown in Sections 3 and 4 below, the PM approach introduces a novel variational perspective on the closure problem exploiting manifolds which allows us to unify within a natural framework previous concepts such as the slow manifold [37] or other notions of *approximate inertial manifolds* [17,57,58], as well as the "fuzzy manifold" [41,65,68] or "quasi manifold" [22]. This variational approach can even be made rigorous as shown in Appendix A. Theorem A.1, proved therein, shows indeed that an optimal PM always exists and that it is the optimal manifold that averages out the fast oscillations, i.e. the best fuzzy manifold one can ever hope for in a certain sense. Detailed numerical computations and rigorous error estimates (see Proposition 3.1) as well as comparison with other natural manifolds such as that associated with the Quasigeostrophic (QG) balance (see Section 4.2), show that the manifold underlying the BE provides a very good approximation of this optimal PM even beyond the criticality, when the fast gravity waves contain a large fraction of the energy.

The framework introduced in this article allows us furthermore to relate the optimal PM to another key object, the *slow conditional expectation*. As explained in Section 4.1 below, the slow conditional expectation provides the best vector field of the space of slow variables that approximates the PE dynamics, and it can be easily derived from the optimal PM (and thus the BE in practice); see (4.7) below. This slow conditional expectation (and thus the optimal PM) becomes however insufficient for closing with only the slow variables, i.e. for ϵ-values beyond ϵ_* for which an explosion of energetic fast oscillations occurs, as explained in Section 4.3. It is shown then that corrective terms are needed in such a situation. These terms take the form of integral terms accounting for the cross-interactions between the slow and fast variables that the

[1] This point corresponds to the unstable equilibrium of the pendulum and the neutral equilibrium of the harmonic oscillator.

[2] This point is an hyperbolic equilibrium of the LK system, a property that allows for the application of the standard Hartman-Grobman theory which can be furthermore combined with the Siegel's linearization theory [1] to infer rigorously to the existence of a local slow manifold; see [15].

Please cite this article as: M.D. Chekroun et al., The emergence of fast oscillations in a reduced primitive equation model and its implications for closure theories, Computers and Fluids (2016), http://dx.doi.org/10.1016/j.compfluid.2016.07.005

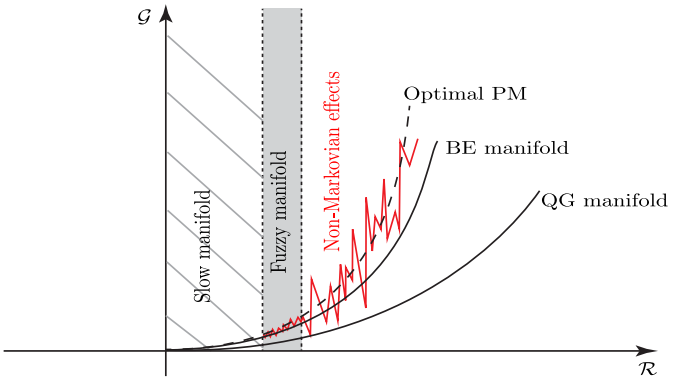

Fig. 1. A revised schematic of Leith's Fig. 1 in [37]. $\mathscr{R}$ and $\mathscr{G}$ are respectively, rotational (y_i, z_i)- and gravitational x_i-modal amplitudes. The origin is associated with $\epsilon \to 0$. The QG manifold can be identified with Leith's slow nonlinear first approximation $\mathscr{M}_1$, and the other manifolds drawn here are explained in this article. Non-Markovian and stochastic effects have to be included in the closure of the slow variables when $\epsilon \geq \epsilon_*$ and explosions of fast (energetic) oscillations take place; see Section 4.3.

optimal PM cannot parameterize (as a minimizer) and involve the past of the slow variables, leading thus to *non-Markovian (i.e. memory) effects*. The iconic Leith's Fig. 1 [37] can then be revisited under this new unified understanding of this still open problem when an explosion of fast (energetic) oscillations occurs; see Fig. 1.

2. The Lorenz 9D model from the primitive equations and the emergence of fast oscillations

2.1. The original model

The model that we analyze hereafter is the nine-dimensional system of ODEs initially derived by Lorenz in [40] as a truncation of the Primitive Equations onto three Fourier spatial basis functions:

$$a_i \frac{dx_i}{d\tau} = a_i b_i x_j x_k - c(a_i - a_k)x_j y_k + c(a_i - a_j)y_j x_k - 2c^2 y_j y_k - \nu_0 a_i^2 x_i + a_i(y_i - z_i), \tag{2.1a}$$

$$a_i \frac{dy_i}{d\tau} = -a_k b_k x_j y_k - a_j b_j y_j x_k + c(a_k - a_j)y_j y_k - a_i x_i - \nu_0 a_i^2 y_i, \tag{2.1b}$$

$$\frac{dz_i}{d\tau} = -b_k x_j (z_k - h_k) - b_j (z_j - h_j)x_k + c y_j (z_k - h_k) - c(z_j - h_j)y_k + g_0 a_i x_i - \kappa_0 a_i z_i + F_i. \tag{2.1c}$$

The above equations are written for each cyclic permutation of the set of indices (1, 2, 3), namely, for

$$(i, j, k) \in \{(1, 2, 3), (2, 3, 1), (3, 1, 2)\}. \tag{2.2}$$

The parameters are chosen such that

$$\begin{aligned} &a_1 = a_2 = 1, \ a_3 = 3, \\ &\nu_0 = \kappa_0 = \frac{1}{48}, \ g_0 = 8, \\ &b_i = (a_i - a_j - a_k)/2, \\ &c = \sqrt{b_1 b_2 + b_2 b_3 + b_3 b_1}, \\ &h_1 = -1, \ h_2 = h_3 = F_2 = F_3 = 0. \end{aligned} \tag{2.3}$$

These values of the parameters are those used in the Lorenz's original paper [40]; see also [27]. Our analysis of the parameter dependence of the dynamics is performed on a rescaled version of the (2.1) that we present next.

2.2. The rescaled version

A formal rescaling of (2.1) is performed with the following definitions:

$$\begin{aligned} &t = \epsilon \tau, \quad (N_0, K_0) = (\nu_0, \kappa_0)/\epsilon, \quad \mathscr{F}_i = F_i/\epsilon^2, \\ &(Y_i, Z_i) = (y_i, z_i)/\epsilon, \quad X_i = x_i/\epsilon^2, \quad H_i = h_i/\epsilon. \end{aligned} \tag{2.4}$$

The purpose is to reformulate (2.1) such as a separation of time scales between fast and slow evolution becomes explicit. With these definitions the system (2.1) becomes

$$\begin{aligned} \epsilon^2 a_i \frac{dX_i}{dt} &= \epsilon^3 a_i b_i X_j X_k - \epsilon^2 c(a_i - a_k)X_j Y_k + \epsilon^2 c(a_i - a_j)Y_j X_k \\ &\quad - 2\epsilon c^2 Y_j Y_k - \epsilon^2 N_0 a_i^2 X_i + a_i(Y_i - Z_i), \\ a_i \frac{dY_i}{dt} &= -\epsilon a_k b_k X_j Y_k - \epsilon a_j b_j Y_j X_k + c(a_k - a_j)Y_j Y_k \\ &\quad - a_i X_i - N_0 a_i^2 Y_i, \\ \frac{dZ_i}{dt} &= -\epsilon b_k X_j (Z_k - H_k) - \epsilon b_j (Z_j - H_j)X_k + c Y_j (Z_k - H_k) \\ &\quad - c(Z_j - H_j)Y_k + g_0 a_i X_i - K_0 a_i Z_i + \mathscr{F}_i. \end{aligned} \tag{2.5}$$

In (2.5), the time t is an $\mathscr{O}(1)$ slow time; (X, Y, Z) are $\mathscr{O}(1)$ amplitudes for the divergent velocity potential, streamfunction, and dynamic height, respectively. In this setting N_0 and K_0 are rescaled damping coefficients in the slow time. The $\mathscr{F}_i$ are $\mathscr{O}(1)$ control parameters that, in combination with variations of ϵ, can be used to effect regime transitions/bifurcations. In a general way ϵ can be identified with the Rossby number.

In fact the Lorenz's quasigeostrophic system [39] and Leith's slow manifold [37] can be recovered by setting $\epsilon = 0$ in (2.5). Indeed after setting $\epsilon = 0$ and multiplying the Y-equations by g_0, one obtains by addition with the Z-equations:

$$(a_i g_0 + 1)\frac{dY_i}{dt} = g_0 c(a_k - a_j)Y_j Y_k - a_i(a_i g_0 N_0 + K_0)Y_i - c H_k Y_j + c H_j Y_k + \mathscr{F}_i. \tag{2.6}$$

written again for each cyclic permutation (i, j, k) of (1, 2, 3). Transforming this system back to the original variables and performing now the change of variables such as in [40, Eqs. (44)–(47)], one obtains the famous Lorenz 1963 model of [39].

Solutions of higher-order accuracy in $\epsilon > 0$ that are entirely slow in their evolution are, by definition, balanced solutions, and [27] showed by construction several examples of explicitly specified, approximate balanced models. One of these, the Balance Equations (BE), was conspicuously more accurate than the others when judged in comparison with apparently slow solutions of (2.1).[3]

In the absence of nonlinear terms, each of the i modes is independent of the others. Fast oscillations are to be identified as $\mathscr{O}(1/\epsilon)$ in frequency: the rest-state, flat-topography (i.e. h-variables constant), unforced, undamped, inertia-gravity oscillations satisfy a slow-time dispersion relation with

$$\omega_i^2 = \epsilon^{-2}(1 + g_0 a_i). \tag{2.7}$$

Note that the minimum frequency magnitude $|\omega|$ is $\epsilon^{-1} \gg 1$.

The initialization problem addressed by Leith [37] and others is how to define (X_i, Y_i, Z_i) at $t = 0$ such that for finite ϵ the evolution remains slow for an $\mathscr{O}(1)$ slow time.

[3] The nonlinear Balance Equations are one of many proposals for the apparently dominant, slowly evolving component of many atmospheric and oceanic flows that emerged during the latter part of the 20th century. It is based on a minimalistic simplification of the horizontal momentum curl and divergence equations, plus hydrostatic balance, motivated by a consistent $\mathscr{O}(\epsilon)$-approximation to the PE [45]. We refer to Sect. 3 below for further mathematical and numerical discussion on the BE.

Please cite this article as: M.D. Chekroun et al., The emergence of fast oscillations in a reduced primitive equation model and its implications for closure theories, Computers and Fluids (2016), http://dx.doi.org/10.1016/j.compfluid.2016.07.005

Transitions to chaos are achieved with increasing $|F_i|$ [39]. The "slow manifold" is achieved at $\epsilon = 0$ for fixed $\mathscr{F}_i$. The central scientific question is when and how in $(\epsilon, \mathscr{F}_i)$ fast oscillations spontaneously emerge and persist (or at least recur) when the $\mathscr{F}_i(t)$ are entirely slow functions (*e.g.*,a constant). Ancillary questions, addressed partly in [27], are whether BE and other approximate balanced models' solutions remain entirely slow for all parameters, where they cease to be integrable in time, and whether their accuracy, relative to solutions of (2.1), fails before slowness fails. In the present paper this question is further generalized to one of devising optimal closures (parameterizations) for representing PE solutions, either when it has only a slow behavior or a combined fast+slow behavior.

2.3. Smooth and abrupt emergence of fast oscillations: ϵ-dependence

For the parameter-dependence experiments reported below, the rescaled model (2.5) has been numerically integrated using a standard fourth-order Runge–Kutta (RK4) method. Throughout the numerical experiments, we have taken the initial data to be very close to the Hadley fixed point. Recall that the Hadley fixed point is given by (cf. [27, Eq. (33)])

$$\begin{aligned} y_1 &= \frac{F_1}{a_1\nu_0(1+a_1g_0+\nu_0^2a_1^2)},\\ x_1 &= -\nu_0 a_1 y_1,\\ z_1 &= (1+\nu_0^2a_1^2)y_1,\\ x_2 &= x_3 = y_2 = y_3 = z_2 = z_3 = 0. \end{aligned} \tag{2.8}$$

The initial data we used for integrating Eq. (2.5) is taken by setting $y_1 = F_1/(a_1\nu_0(1+a_1g_0))$, $z_1 = y_1$, $y_2 = -10^{-5}$ and $z_2 = 10^{-5}$ while keeping the other components equal to those corresponding to the Hadley fixed point, followed by a rescaling in the (X, Y, Z)-variable. Given the parameter values recalled in (2.3), this initial datum in the (x, y, z) coordinates is very close to that used to initialize the PE (2.1) in [27] and provides thus a complimentary dataset to study parameter-dependence.

The numerical experiments have been carried out for the ϵ-value in the range [0.2236, 1.9748], with $\mathscr{F}_1$ fixed to be 0.1. This setting corresponds to a range of F_1 given by [0.005, 0.39], which is essentially the range of F_1 values explored in [27]. Note that the PE solution blows up in finite time for F_1 above 0.40 as noted in [27]. After an initial pruning experiment consisting of 150 ϵ-values equally spaced in the interval [0.2236, 1.9748], local refinements in the ϵ-mesh are then performed for the following three intervals

- $I_1 = [0.7172, 0.72899]$,
- $I_2 = [1.034, 1.14]$,
- $I_3 = [1.5518, 1.5632]$.

The local refinements within these intervals are made in order to better resolve the dynamical transitions that take place in each of them and whose the main transition of interest, given the scope of this article, arises in I_3 as discussed below.[4] Respectively 50, 50 and 30 equally spaced ϵ-values are added as a refinement of these intervals, leading to a total of 280 ϵ-values. For each of these ϵ-values, the simulation of the rescaled model (2.5) is then performed for $2\times10^5 + 4\times10^6$ time steps, starting the integration from the aforementioned perturbation of the Hadley fixed point with a time step size δt fixed to be 1/240. The parameter-dependence experiments are then conducted below for $N = 4\times10^6$ data points, resulting from a removal of the first 2×10^5 data points aimed for the removal of some transient adjustment.

Within this numerical set-up and for the available ϵ-values, the total variation (TV) of each component u_j ($u = X$, Y or Z, $j \in \{1, 2, 3\}$) of the solution to Eq. (2.5) has then been evaluated as follows

$$\|u_j\|_{\mathrm{TV}} = \sum_{k=0}^{M-1} \Big| u_j((k+1)\delta t(\epsilon)) - u_j(k\delta t(\epsilon)) \Big|, \tag{2.9}$$

where the time-increment $\delta t(\epsilon)$ is chosen so that it corresponds to an hourly sampling in the original physical time τ and M denotes the corresponding nearest integer to $N/\delta t(\epsilon)$. The results are shown in Fig. 2. As it can be observed in Fig. 2, a sharp transition is manifested as ϵ crosses a critical value $\epsilon_* \approx 1.5522$, marked by a dash line on this figure. This transition as observed on this metric, corresponds to an actual abrupt *dynamical transition* of the system's long-term dynamics as reflected at the model's statistical behavior by looking at the variation of the power spectral density (PSD) of each of the model's components across the transition; see Fig. 3. In the time-domain this transition is manifested by a spontaneous generation of "explosive" fast oscillations on the X- and Z-variables as described below and shown in Fig. 4 for X_2. This is also reflected in the energy balance shown in the center and right panels of Fig. 5.

For the range of ϵ-values considered here (associated with $\mathscr{F}_1 = 0.1$), we have performed complimentary cross-checking analysis (based on PSD and Lyapunov exponents analysis such as used in e.g. [52]) and distinguished essentially five distinct regimes that are marked by the color coding as indicated in Fig. 2 and in other figures hereafter. These regimes can be roughly grouped as follows, besides the stable attractive steady states observed for smaller ϵ-values than those shown in Fig. 2 and corresponding to the F_1-values of [27], after rescaling; see also [62].

(I) **Periodic/quasi-periodic behaviors.** For ϵ sufficiently large (corresponding roughly to the ϵ-values located between blue and the cyan dots of Fig. 2), periods reflecting the propagation of Rossby waves in this low-dimensional PE model may emerge such as a 7-day dominant period (in the original time τ) for the X_j-,Y_j- and Z_j-variables ($j \in \{2, 3\}$), and a 3.5-day period for X_1-,Y_1- and Z_1-variables.

(II) **Slow chaos.** It corresponds to ϵ-values in which no fast oscillations develop. Although $\epsilon \neq 0$, these ϵ-values correspond to solution profiles whose Y-components form attractors of reminiscent shape with the famous Lorenz 1963 attractor [39] (e.g. Fig. 7), but with non-trivial departures from the QG solutions at finite ϵ, which therefore can be called "balanced".

(III) **Fast but small-amplitude oscillations and no chaos**. Here these fast oscillations are characteristic of inertia-gravity waves and are typically superimposed on solution profiles dominated by the 7-day or the 3.5-day period. A typical example of such a solution is displayed in the upper-left panel of Fig. 4 for $\epsilon = 1.5518$. In this regime, the emergence of fast oscillations is smooth but non-monotonic as ϵ increases (not shown). The fraction of energy contained in the X-variables does not exceed 5% for this regime; see cyan dots in the center panel of Fig. 5.

(IV) **Regimes of spontaneous generation of "explosive" fast oscillations on the X- and Z-variables when a $\epsilon \geq \epsilon_*$.** By explosive, we mean that these fast oscillations can experience bursting periods of time with amplitudes up to one order of magnitude larger than the magnitude of the slow oscillations preceding the transition; for a typical example, see the panel corresponding to $\epsilon = 1.5536$ in Fig. 4. Fig. 3 shows that these bursts correspond to the emergence of a broad-band peak in the PSD located around 4 day^{-1} for $\epsilon = \epsilon_*$ although more energetic for the fast X-variables (and Z-variables (not shown)) than

[4] In sharp contrast with the transition happening in I_3, those arising in I_1 and I_2 are more standard transitions between periodic/quasi-periodic and chaotic regimes, in which no fast oscillations develop.

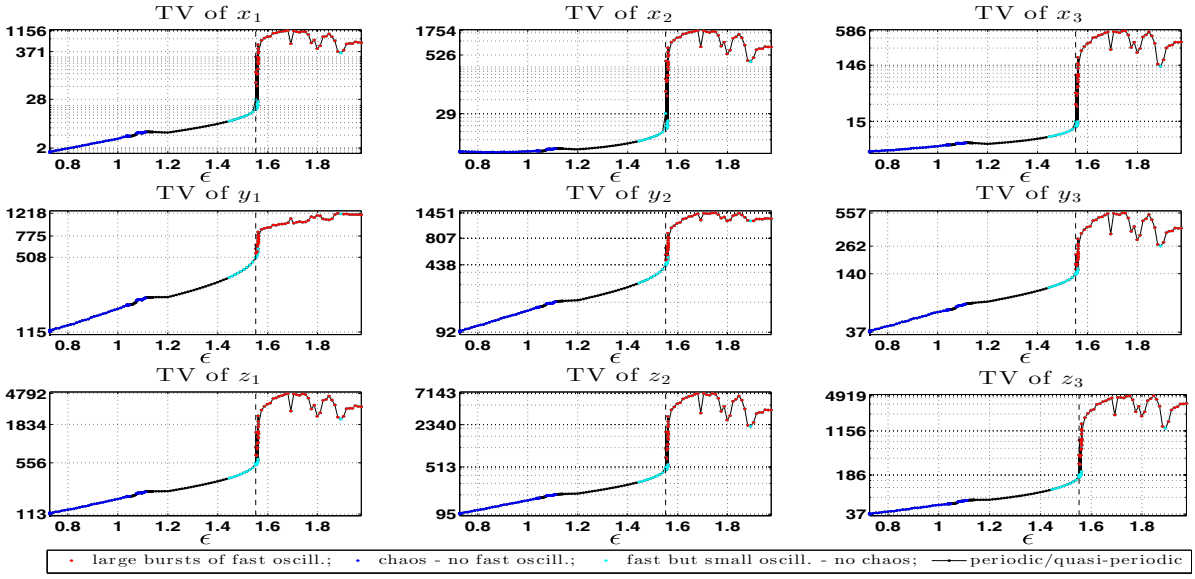

Fig. 2. ϵ-dependence of the total variation (TV) (2.9) for the *X*-,*Y*-, and *Z*-variables (semilogarithmic scales). The first ϵ-value (referred hereafter as ϵ_*) for which explosive bursts of fast oscillations appear is marked by the dashed line, it corresponds to a jump in TV for each variable. See text for further details about the legend. Semilogarithmic scales are used here.

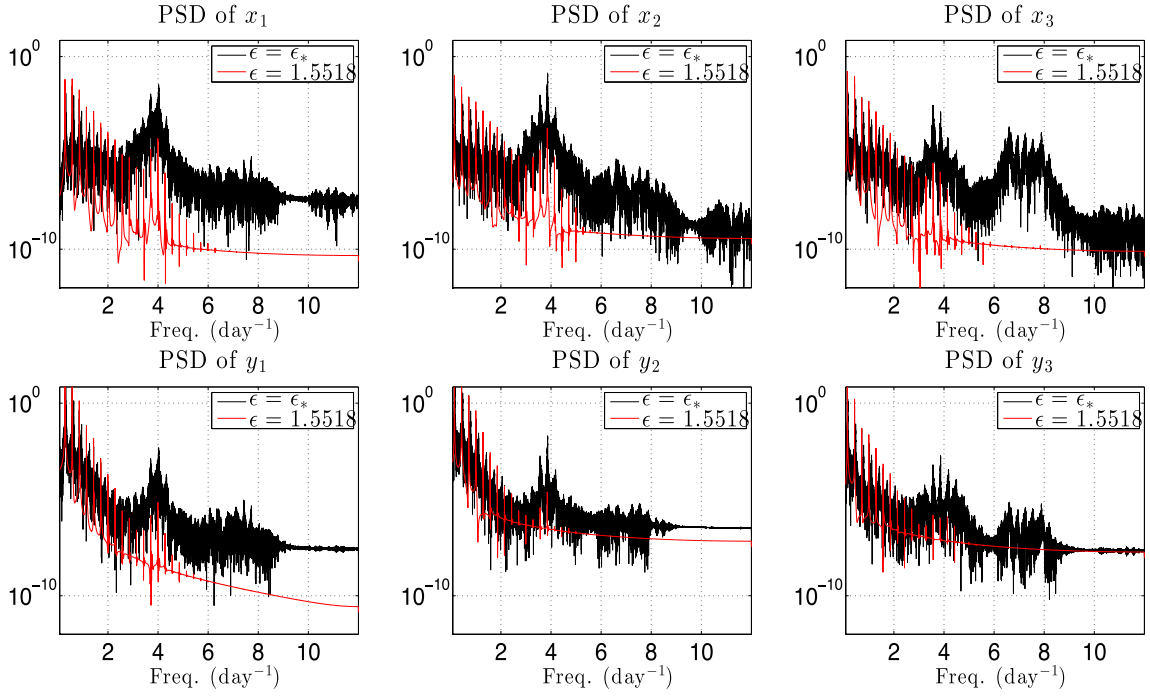

Fig. 3. Variation of the power spectral density (PSD) across the transition (semilogarithmic scales). For each variable, the emergence of a broad-band peak located around 4 day^{-1} is clearly visible for $\epsilon = \epsilon_*$ although more energetic for the fast *X*-variables than for the slow *Y*-variables. These peaks correspond to the emergence of a 6*h*-period oscillations associated with inertia-gravity waves, that can become very energetic in the course of time; see Fig. 4 and center-panel of Fig. 5. Similar behaviors than for the *Z*-variables have been observed. For $\epsilon = 1.5518$ (right below ϵ_*) the dominant oscillation is approximately of a 7-day period (Rossby waves, with their harmonics), but a local deformation of the PSD (more visible for the *X*-variables) located around 4 day^{-1} is observed. This local deformation corresponds to small amplitude fast oscillations as shown in the upper-left panel of Fig. 4.

for the slow *Y*-variables. These peaks correspond to the emergence of a 6*h*-period oscillations associated with inertia-gravity waves that can become very energetic in the course of time; see Fig. 4 and right-panel of Fig. 5. For $\epsilon = 1.5518$ (right below ϵ_*) the dominant oscillation is approximately of a 7-day period (Rossby waves, with their harmonics), but a local deformation of the PSD (more visible for the *X*-variables) that peaks around 4 day^{-1} (6h), is observed. This local deformation of the PSD corresponds to small-amplitude fast oscillations as shown in the upper-left panel of Fig. 4. A comparison of the PSDs of the *Y*-variables with those of the *X*-variables at ϵ_* provides evidence that fast oscillations are however comparatively less energetic for the *Y*-variables.

Please cite this article as: M.D. Chekroun et al., The emergence of fast oscillations in a reduced primitive equation model and its implications for closure theories, Computers and Fluids (2016), http://dx.doi.org/10.1016/j.compfluid.2016.07.005

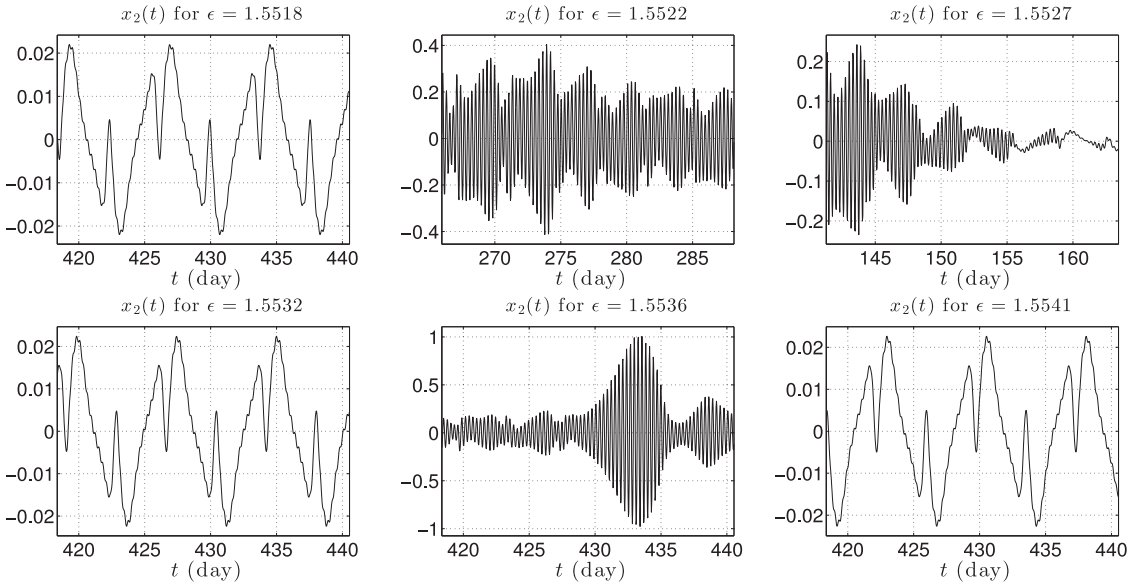

Fig. 4. Solution profiles of x_2 across the "grey-zone." The ϵ-value 1.5522 corresponds to the critical ϵ_* for which burst of fast oscillations have been first observed (after transient removed). The three ϵ-values for which small fast oscillations are superimposed on an approximate 7-day oscillation (i.e. $\epsilon = 1.5518$; $\epsilon = 1.5532$; and $\epsilon = 1.5541$) do not display burst episodes for later times. For the other ϵ-values displayed here, bursts develop at later stage than shown.

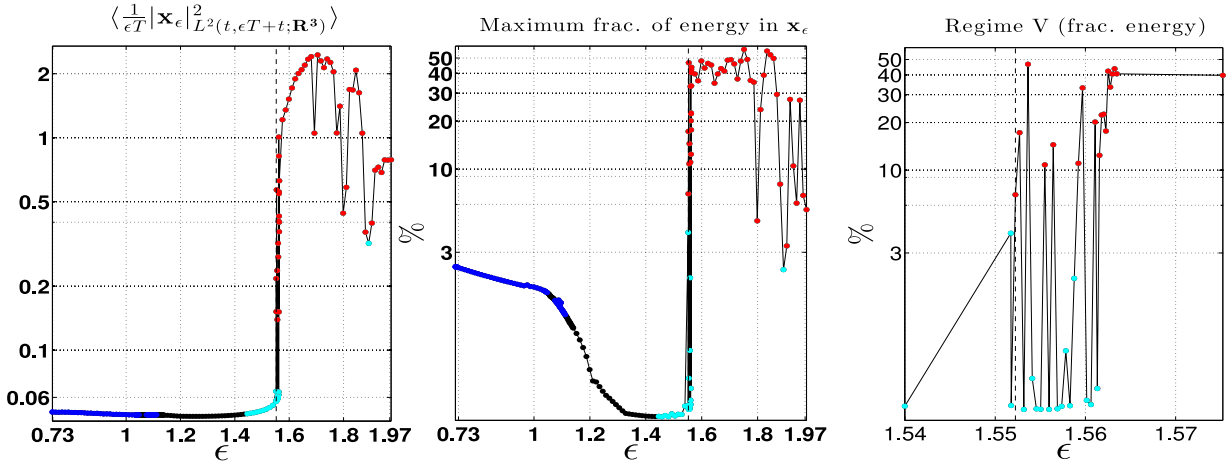

Fig. 5. Left panel: Mean energy, $\langle \frac{1}{\epsilon T} |\mathbf{x}_\epsilon|^2_{L^2(t,\epsilon T+t;\mathbb{R}^3)} \rangle$, contained in $\mathbf{x}_\epsilon = (X_1, X_2, X_3)$ in Eq. (2.5). Here ϵT corresponds to 10 days in the original time τ. Center panel: For each ϵ, the maximum fraction of energy (in %) contained in $\mathbf{x}_\epsilon$ in the course of time is reported. Right panel: Maximum fraction of energy contained in $\mathbf{x}_\epsilon$ as Regime V is crossed. In each panel, the vertical dash line emanates from $\epsilon = \epsilon_*$ and the color coding is the same as in Fig. 2.

These burst episodes of fast oscillations are typically followed in time by quiet episodes in which the fast oscillations are still present but become of much smaller amplitudes and are superimposed on an average motion which resembles that of solutions for the ϵ-value right below ϵ_* (similar as in the upper-left panel of Fig. 4) and that is close to the quasi-geostrophic limit cycle (shown in [68, Fig. 2] for the (Y_2, Y_3)-projection). As time evolves, the episodes of energetic bursts of fast oscillations may reappear in an on-off intermittent way.

Noteworthy within this regime is the case $\epsilon = 1.9043$ [5] for which the amplitudes of fast variables are of an energy level intermediate between those of Regime III and the aforementioned bursts; compare the upper-panel of Fig. 10 with the upper-panels of Figs. 8 and 9 (see also Fig. 5).

(V) **"Grey zone."** It corresponds roughly to ϵ-values in the tiny interval $[\epsilon_*, 1.5632]$ with $\epsilon_* \approx 1.5522$ denoting the first ϵ-value[6] in which spontaneous generation of explosive fast oscillations has been observed; see upper-center panel in Fig. 4. Within this tiny interval, two very close ϵ-values can either belong to Regime III or Regime IV; see right panel of Fig. 5. As illustrated in Fig. 4 and expressed in term of energy balance (see right panel of Fig. 5), this interlacing of dynamical behaviors is non-monotonic as ϵ increases. In particular, it rules out a simple functional dependence (exponential or others) regarding the settlement and growth of fast oscillations as ϵ increases.

Thus, a sharp dynamical transition occurring for $\epsilon = \epsilon_*$, at the interface between Regime III and Regime IV, has been identified in the rescaled PE (2.5) and therefore in the original PE (2.1), after rescaling. This transition corresponds to the emergence of fast

[5] Distinguishable in e.g. the center panel of Fig. 5 as the immediate red dot located to the right of the cyan dot isolated in the "red sea." This zone deserves an ϵ-mesh refinement that will be performed elsewhere.

[6] According to our (variable) ϵ-mesh resolution such as described above, the best approximation of ϵ_* we found is given by 1.552239833273196.

gravity waves that can contain a significant fraction of the energy (up to $\sim$ 40%) as time evolves and that can either populate transient behaviors of various lengths or survive in an intermittent way as both time flows and ϵ varies beyond ϵ_*. The parameter-dependence of the dynamical behavior presented above is consistent with that of [27], except for the identification of Regimes III, IV and V, which results here from an intensive probing in the ϵ-direction and longer numerical simulations (with smaller time-steps) than originally computed in [27]; see however [62] for examples in Regimes III and IV. Note that when the initial datum of [27] is used, the aforementioned regime classification still holds with bursts of fast oscillations occurring though at different time instances for Regime IV and V, as well as slightly perturbed ϵ-location.

Although from a mathematical viewpoint the transition occurring at $\epsilon = \epsilon_*$ is a quasi-periodic-to-chaos transition, its precise characterization needs further clarification from a dynamical perspective. Postponing for another occasion such an analysis at the transition, we propose below to study the implications of the existence of such a critical transition on the closure problem from the slow variables. For that purpose we revisit the Balance Equations (BE) within the framework of parameterizing manifolds introduced in [9,12] for different but related parameterization objectives.

3. The balance equations across the critical transition

3.1. The balance equations as a slow manifold closure

As initially proposed in [27], we present hereafter the BE and its derivation from the original Lorenz model (2.1). (The original derivation was motivated by the formulation of the BE as a "balanced" approximation to the PE as fully 3D PDE systems.) The presentation here is made in the original variables in (2.1), the rescaled version being obvious; see Section 3.2.

Numerical simulations of Eq. (2.5) show that the variable $\mathbf{x} := (x_1, x_2, x_3)$ carries only a small fraction of the total energy for $\epsilon < \epsilon_*$; see Fig. 5. This quantitative remark indicates (after rescaling) that dropping the terms involving x_i, x_j, and x_k from the right-hand side (RHS) of Eq. (2.1a) should not be detrimental — at least for $\epsilon < \epsilon_*$ — to model the evolution of $\mathbf{x}$, namely that the latter could be reasonably approximated by

$$a_i \frac{dx_i}{d\tau} = -2c^2 y_j y_k + a_i(y_i - z_i). \tag{3.1}$$

This equation corresponds also to retaining the terms of order less than or equal to ϵ in Eq. (2.5), leading to the BE model (3.10) as explained hereafter[7].

Assuming furthermore that the terms on the RHS of this latter equation are balanced in the sense that the time average of $\frac{dx_i}{d\tau}$ is small, one can propose the following surrogate of (3.1):

$$-2c^2 y_j y_k + a_i(y_i - z_i) = 0. \tag{3.2}$$

The Eq. (3.2) together with (2.1b) and (2.1c) constitute the so-called *balance equations* (BE) originally proposed in [27]. Namely, the BE are given by the following system of *differential-algebraic equations (DAEs)*

$$-2c^2 y_j y_k + a_i(y_i - z_i) = 0, \tag{3.3a}$$

$$a_i \frac{dy_i}{d\tau} = -a_k b_k x_j y_k - a_j b_j y_j x_k + c(a_k - a_j) y_j y_k - a_i x_i - \nu_0 a_i^2 y_i, \tag{3.3b}$$

$$\frac{dz_i}{d\tau} = -b_k x_j (z_k - h_k) - b_j (z_j - h_j) x_k + c y_j (z_k - h_k) - c(z_j - h_j) y_k + g_0 a_i x_i - \kappa_0 a_i z_i + F_i, \tag{3.3c}$$

written again for each cyclic permutation of (1, 2, 3).

The main interest of this system of DAEs relies on its reduction to a three-dimensional system of ODEs in the variable $\mathbf{y} := (y_1, y_2, y_3)$, provided that a solvability condition (conditioned itself on $\mathbf{x}$ and $\mathbf{z}$) is satisfied. To proceed to such a reduction we first note that (3.3a) provides a parameterization of $\mathbf{z} := (z_1, z_2, z_3)$ in terms of $\mathbf{y}$, namely

$$z_i = G_i(\mathbf{y}) = y_i - \frac{2c^2}{a_i} y_j y_k. \tag{3.4}$$

The parameterization of $\mathbf{x}$ in terms of $\mathbf{y}$ can be then obtained by following the two-step procedure of [27]. First, by taking the time derivative on both sides of (3.3a), we naturally obtain

$$-2c^2 \left(\frac{dy_j}{d\tau} y_k + y_j \frac{dy_k}{d\tau} \right) + a_i \left(\frac{dy_i}{d\tau} - \frac{dz_i}{d\tau} \right) = 0. \tag{3.5}$$

The substitution of the derivative terms in (3.5) by using (3.3b) and (3.3c), leads then after simplification to (cf. [27, Eq. (30)]):

$$\begin{aligned}
&x_i[a_i a_j a_k (1 + g_0 a_i) - 2c^2 (a_j^2 b_j y_j^2 + a_k^2 b_k y_k^2)] \\
&\quad - x_j[a_j a_k (y_k (2c^2 - a_k b_k) + a_i b_k (z_k - h_k)) + 2c^2 a_i a_j b_i y_i y_j] \\
&\quad - x_k[a_j a_k (y_j (2c^2 - a_j b_j) + a_i b_j (z_j - h_j)) + 2c^2 a_i a_k b_i y_i y_k] \\
&= a_j a_k[c(a_k - a_j) y_j y_k + c a_i ((z_j - h_j) y_k - y_j (z_k - h_k)) \\
&\quad + a_i (\nu_0 a_i (z_i - y_i) - F_i)] \\
&\quad - 2c^2[c a_j (a_j - a_i) y_i y_j^2 + c a_k (a_i - a_k) y_i y_k^2 \\
&\quad - \nu_0 a_j a_k (a_j + a_k) y_j y_k].
\end{aligned} \tag{3.6}$$

The above algebraic system of equations can be written into the following compact form:

$$M(\mathbf{y}, \mathbf{z})\mathbf{x} = \begin{pmatrix} \Delta_{1,2,3}(\mathbf{y}) & \Gamma_{1,2,3}(\mathbf{y}, \mathbf{z}) & \Sigma_{1,2,3}(\mathbf{y}, \mathbf{z}) \\ \Sigma_{2,3,1}(\mathbf{y}, \mathbf{z}) & \Delta_{2,3,1}(\mathbf{y}) & \Gamma_{2,3,1}(\mathbf{y}, \mathbf{z}) \\ \Gamma_{3,1,2}(\mathbf{y}, \mathbf{z}) & \Sigma_{3,1,2}(\mathbf{y}, \mathbf{z}) & \Delta_{3,1,2}(\mathbf{y}) \end{pmatrix} \begin{pmatrix} x_1 \\ x_2 \\ x_3 \end{pmatrix} = \begin{pmatrix} d_{1,2,3}(\mathbf{y}, \mathbf{z}) \\ d_{2,3,1}(\mathbf{y}, \mathbf{z}) \\ d_{3,1,2}(\mathbf{y}, \mathbf{z}) \end{pmatrix}, \tag{3.7}$$

with

$$\begin{aligned}
\Delta_{i,j,k}(\mathbf{y}) &= a_i a_j a_k (1 + g_0 a_i) - 2c^2 (a_j^2 b_j y_j^2 + a_k^2 b_k y_k^2), \\
\Gamma_{i,j,k}(\mathbf{y}, \mathbf{z}) &= -\Big[a_j a_k (y_k (2c^2 - a_k b_k) + a_i b_k (z_k - h_k)) \\
&\qquad + 2c^2 a_i a_j b_i y_i y_j \Big], \\
\Sigma_{i,j,k}(\mathbf{y}, \mathbf{z}) &= -\Big[a_j a_k (y_j (2c^2 - a_j b_j) + a_i b_j (z_j - h_j)) \\
&\qquad + 2c^2 a_i a_k b_i y_i y_k \Big], \\
d_{i,j,k}(\mathbf{y}, \mathbf{z}) &= a_j a_k[c(a_k - a_j) y_j y_k + c a_i ((z_j - h_j) y_k \\
&\qquad - y_j (z_k - h_k)) + a_i (\nu_0 a_i (z_i - y_i) - F_i)] \\
&\qquad - 2c^2[c a_j (a_j - a_i) y_i y_j^2 + c a_k (a_i - a_k) y_i y_k^2 \\
&\qquad - \nu_0 a_j a_k (a_j + a_k) y_j y_k],
\end{aligned} \tag{3.8}$$

for which (i, j, k) denotes once more any cyclic permutation of (1, 2, 3).

Now provided that the 3 × 3 matrix $M(\mathbf{y}, \mathbf{z})$ in (3.7) is invertible,[8] i.e. $\det(M(\mathbf{y}, \mathbf{z})) \neq 0$, one obtains (implicitly) $\mathbf{x}$ as a function

[7] See also [28] for an alternative Hamiltonian version of the BE (from the full PE) by expanding an Hamilton's principle for the PE in powers of the Rossby number, $\epsilon \ll 1$, truncating at order $\mathcal{O}(\epsilon)$, then retaining all the terms that result from taking variations.

[8] We refer to [48] for a characterization of critical conditions for the limits of balance in the context of full PE. In that context, the breakdown of the solvability

Φ of $\mathbf{y}$ given by

$$\Phi(\mathbf{y}) = (\Phi_1(\mathbf{y}), \Phi_2(\mathbf{y}), \Phi_3(\mathbf{y})) = \big[M(\mathbf{y}, G(\mathbf{y}))\big]^{-1} \begin{pmatrix} d_{1,2,3}(\mathbf{y}, G(\mathbf{y})) \\ d_{2,3,1}(\mathbf{y}, G(\mathbf{y}))) \\ d_{3,1,2}(\mathbf{y}, G(\mathbf{y}))) \end{pmatrix}, \tag{3.9}$$

where $G(\mathbf{y})$ is the vector-valued function whose components G_i ($i \in \{1, 2, 3\}$) are given in (3.4). The function Φ will be referred hereafter as the *BE manifold*, it is aimed to provide a slaving relationship between $\mathbf{x}$ and $\mathbf{y}$.

With Φ given by (3.9) (provided that $\det(M(\mathbf{y}, \mathbf{z})) \neq 0$), Eq. (3.3b) can now be written in a closed form of the $\mathbf{y}$-variable, i.e.:

$$a_i \frac{\mathrm{d}y_i}{\mathrm{d}\tau} = -a_k b_k \Phi_j(\mathbf{y}) y_k - a_j b_j y_j \Phi_k(\mathbf{y}) + c(a_k - a_j) y_j y_k - a_i \Phi_i(\mathbf{y}) - \nu_0 a_i^2 y_i, \tag{3.10}$$

providing the aforementioned three-dimensional system of ODEs.

Although this reduced system of the original PE model (2.1) is based on the heuristic approximation (3.2), we provide in the next section rigorous error estimates that show the validity of this heuristic for $\epsilon < \epsilon_*$. These error estimates show furthermore that even for certain $\epsilon \geq \epsilon_*$ corresponding to a violation of the "small-fraction of energy" assumption used in the derivation of the BE-model (3.10), the PE slow rotational variable $\mathbf{y}$ may be still reasonably well mimicked, in an average sense, by its BE surrogate; see Fig. 9 and related discussion below. At the same time, the critical value ϵ_* characterizes a breakdown of the slaving principle (or any of its approximate/fuzzy versions), as explained below.

3.2. Parameterization defect, modeling error estimates and breakdown of slaving principles

In this section we derive error estimates following ideas used in [9] about *finite-horizon parameterizing manifolds* introduced in the context of optimal control of nonlinear partial differential equations (PDEs); see also [12].

Recall the BE model (3.10) derived in the previous section. In order to compare the dynamics from BE with that from the rescaled PE, we will transform the BE solutions and the BE manifold according to the scalings

$$\mathbf{y}_\epsilon = \frac{\mathbf{y}}{\epsilon}, \text{ and } \Phi_\epsilon(\mathbf{y}_\epsilon) = \frac{\Phi(\mathbf{y})}{\epsilon^2}, \tag{3.11}$$

respectively.

The function Φ_ϵ defines a manifold $\mathscr{M}_\epsilon$ above the projection on the $\mathbf{y}$-variable of the attractor $\mathscr{A}_\epsilon$ according to

$$\mathscr{M}_\epsilon := \left\{ \sum_{i=1}^3 \xi_i e_{i+3} + \sum_{i=1}^3 \Phi_{\epsilon,i}(\xi) e_i : \xi = \sum_{i=1}^3 \xi_i e_{i+3} \in \Pi_{\mathfrak{s}} \mathscr{A}_\epsilon \right\}. \tag{3.12}$$

We will also make use of the following convex set:

$$\mathscr{N}_\epsilon = \mathrm{conv}\Big(\mathscr{M}_\epsilon \bigcup \Pi_{\mathfrak{f}_1+\mathfrak{s}} \mathscr{A}_\epsilon \Big), \tag{3.13}$$

where for a given bounded set $\mathscr{S}$ in a Euclidean vector space, $\mathrm{conv}(\mathscr{S})$ denotes the convex hull of $\mathscr{S}$, i.e. the minimal convex set containing $\mathscr{S}$.

Here $\Pi_{\mathfrak{s}}$ denotes the projection onto the vector subspace where evolves the slow variable $\mathbf{y}_\epsilon$ namely

$$\mathscr{H}_{\mathfrak{s}} = \mathrm{span}\{e_4, e_5, e_6\}, \tag{3.14}$$

while $\Pi_{\mathfrak{f}_1+\mathfrak{s}}$ denotes the projection onto the vector space of slow-fast variables in which $\mathbf{y}_\epsilon$ and $\mathbf{x}_\epsilon$ evolve, and that is given here by

$$\mathscr{H}_{\mathfrak{f}_1+\mathfrak{s}} = \mathrm{span}\{e_1, e_2, e_3, e_4, e_5, e_6\}. \tag{3.15}$$

Here and above the e_i's denote the canonical vectors of the nine-dimensional Euclidean space.

To this manifold and given $T > 0$, we associate the following *maximum defect of parameterization*

$$Q(\Phi, T, \epsilon) := \max_{t \in [t_1, t_2]} \frac{\int_t^{\epsilon T + t} \big\| \mathbf{x}_\epsilon(t) - \Phi_\epsilon(\mathbf{y}_\epsilon(t)) \big\|^2 \, \mathrm{d}t}{\int_t^{\epsilon T + t} \|\mathbf{x}_\epsilon(t)\|^2 \, \mathrm{d}t}, \tag{3.16}$$

where $[t_1, t_2]$ denotes an interval of integration of (2.5), such that t_1 has been chosen such that transient behavior has been removed and $t_2 > t_1 + \epsilon T$. The time window of integration, ϵT, corresponds to $\frac{T}{8}$ days when converted back to the physical time τ, following again the non-dimensionalization used in [27,40]. We have then the following estimates that provide a measure of the modeling error.

Proposition 3.1. *Given a solution $(\mathbf{x}_\epsilon, \mathbf{y}_\epsilon, \mathbf{z}_\epsilon)$ of the rescaled PE model (2.5) evolving on its global attractor $\mathscr{A}_\epsilon$, the following estimate assesses the modeling error of the slow variable $\mathbf{y}_\epsilon$ by the BE model (3.10):*

$$\int_t^{\epsilon T + t} \left\| \frac{\mathrm{d}\mathbf{y}_\epsilon}{\mathrm{d}t} - \Big(L\mathbf{y}_\epsilon - \Phi_\epsilon(\mathbf{y}_\epsilon) + B_1\big(\mathbf{y}_\epsilon, \mathbf{y}_\epsilon\big) + B_2\big(\mathbf{y}_\epsilon, \Phi_\epsilon(\mathbf{y}_\epsilon)\big) \Big) \right\|^2 \mathrm{d}t \leq (1 + [\mathrm{Lip}(B_2|_{\mathscr{N}_\epsilon})]^2) Q(\Phi, T, \epsilon) |\mathbf{x}_\epsilon|^2_{L^2(t, \epsilon T + t; \mathbb{R}^3)}, \quad t_1 \leq t \leq t_2, \tag{3.17}$$

where

$$L = -\mathrm{diag}(N_0 a_1, N_0 a_2, N_0 a_3), \tag{3.18}$$

and where $B_1\big(\mathbf{y}_\epsilon, \mathbf{y}_\epsilon\big)$ denotes the self-interaction terms between the slow variable $\mathbf{y}_\epsilon$ in the RHS of the y-equation in (2.5) as obtained after division by a_i on both sides. The term $B_2\big(\mathbf{y}_\epsilon, \mathbf{x}_\epsilon\big)$ denotes the cross-interaction between the slow variable $\mathbf{y}_\epsilon$ and the fast variables $\mathbf{x}_\epsilon$.

If one assumes furthermore that the convex set $\mathscr{N}_\epsilon$ (defined in (3.13)) is contained within a ball of radius R centered at the origin, then the Lipschitz constant $\mathrm{Lip}(B_2|_{\mathscr{N}_\epsilon})$ can be controlled by the following upper bound:

$$\mathrm{Lip}(B_2|_{\mathscr{N}_\epsilon}) \leq \epsilon \left[\left(\frac{a_2 b_2}{a_1}\right)^2 + \left(\frac{a_3 b_3}{a_1}\right)^2 + \left(\frac{a_1 b_1}{a_2}\right)^2 + \left(\frac{a_3 b_3}{a_2}\right)^2 + \left(\frac{a_2 b_2}{a_3}\right)^2 + \left(\frac{a_1 b_1}{a_3}\right)^2 \right]^{1/2} R, \tag{3.19}$$

where the a_is and the b_is are the coefficients as in Eq. (2.5).

Proof. Since $(\mathbf{x}_\epsilon, \mathbf{y}_\epsilon, \mathbf{z}_\epsilon)$ is a solution to the rescaled PE model (2.5), it holds that

$$\frac{\mathrm{d}\mathbf{y}_\epsilon}{\mathrm{d}t} = L\mathbf{y}_\epsilon - \mathbf{x}_\epsilon + B_1\big(\mathbf{y}_\epsilon, \mathbf{y}_\epsilon\big) + B_2\big(\mathbf{y}_\epsilon, \mathbf{x}_\epsilon\big). \tag{3.20}$$

The modeling error estimate (3.17) can then be derived by using a straightforward application of a Lipschitz estimate to the cross-interaction nonlinear terms contained in B_2 and the definition of the maximum defect of parameterization $Q(T, \epsilon)$ given by (3.16). Indeed, we have

$$\int_t^{\epsilon T + t} \left\| \frac{\mathrm{d}\mathbf{y}_\epsilon}{\mathrm{d}t} - \Big(L\mathbf{y}_\epsilon - \Phi_\epsilon(\mathbf{y}_\epsilon) + B_1\big(\mathbf{y}_\epsilon, \mathbf{y}_\epsilon\big) + B_2\big(\mathbf{y}_\epsilon, \Phi_\epsilon(\mathbf{y}_\epsilon)\big) \Big) \right\|^2 \mathrm{d}t = \int_t^{\epsilon T + t} \left\| \Phi_\epsilon(\mathbf{y}_\epsilon) - \mathbf{x}_\epsilon + B_2\big(\mathbf{y}_\epsilon, \mathbf{x}_\epsilon\big) - B_2\big(\mathbf{y}_\epsilon, \Phi_\epsilon(\mathbf{y}_\epsilon)\big) \right\|^2 \mathrm{d}t$$

condition coincides with critical conditions for the onset of convection with unstable stratification, for centrifugal instability in parallel and axisymmetric flows, and at least approximately with the onset of strong instabilities in anticyclonic elliptical flows.

$$\leq \int_t^{\epsilon T+t} \left\| \Phi_\epsilon(\mathbf{y}_\epsilon) - \mathbf{x}_\epsilon \right\|^2 \mathrm{d}t + \int_t^{\epsilon T+t} \left\| B_2\left(\mathbf{y}_\epsilon, \mathbf{x}_\epsilon\right) - B_2\left(\mathbf{y}_\epsilon, \Phi_\epsilon(\mathbf{y}_\epsilon)\right) \right\|^2 \mathrm{d}t$$
$$\leq (1 + [\mathrm{Lip}(B_2|_{\mathscr{N}_\epsilon})]^2) \int_t^{\epsilon T+t} \left\| \Phi_\epsilon(\mathbf{y}_\epsilon) - \mathbf{x}_\epsilon \right\|^2 \mathrm{d}t$$
$$\leq (1 + [\mathrm{Lip}(B_2|_{\mathscr{N}_\epsilon})]^2) Q(\Phi, T, \epsilon) |\mathbf{x}_\epsilon|^2_{L^2(t,\epsilon T+t;\mathbb{R}^3)}, \quad t_1 \leq t \leq t_2. \tag{3.21}$$

The bound given in (3.19) for the Lipschitz constant $\mathrm{Lip}(B_2|_{\mathscr{N}_\epsilon})$ can be obtained as follows. Note that by the integral form of the mean value theorem in vector spaces [36, Theorem 4.2], we have

$$B_2\left(\mathbf{y}_\epsilon, \mathbf{x}_\epsilon\right) - B_2\left(\mathbf{y}_\epsilon, \Phi_\epsilon(\mathbf{y}_\epsilon)\right) = \int_0^1 DB_2(\mathbf{y}_\epsilon, s\mathbf{x}_\epsilon + (1-s)\Phi_\epsilon(\mathbf{y}_\epsilon))(\mathbf{x}_\epsilon - \Phi_\epsilon(\mathbf{y}_\epsilon))\,\mathrm{d}s, \tag{3.22}$$

where DB_2 denotes the Jacobian of B_2. It follows that

$$\left\| B_2\left(\mathbf{y}_\epsilon, \mathbf{x}_\epsilon\right) - B_2\left(\mathbf{y}_\epsilon, \Phi_\epsilon(\mathbf{y}_\epsilon)\right) \right\| \leq \left\| \mathbf{x}_\epsilon - \Phi_\epsilon(\mathbf{y}_\epsilon) \right\| \int_0^1 \left\| DB_2(\mathbf{y}_\epsilon, s\mathbf{x}_\epsilon + (1-s)\Phi_\epsilon(\mathbf{y}_\epsilon)) \right\| \mathrm{d}s\,. \tag{3.23}$$

We obtain then:

$$\mathrm{Lip}(B_2|_{\mathscr{N}_\epsilon}) \leq \sup_{(\mathbf{x},\mathbf{y})\in\mathscr{N}_\epsilon} \|DB_2(\mathbf{y},\mathbf{x})\|. \tag{3.24}$$

Recalling that the cross-interaction term B_2 is given by (using the notations in (2.4))

$$B_2(Y,X) = \begin{pmatrix} -\frac{\epsilon a_3 b_3}{a_1} X_2 Y_3 - \frac{\epsilon a_2 b_2}{a_1} Y_2 X_3 \\ -\frac{\epsilon a_1 b_1}{a_2} X_3 Y_1 - \frac{\epsilon a_3 b_3}{a_2} Y_3 X_1 \\ -\frac{\epsilon a_2 b_2}{a_3} X_1 Y_2 - \frac{\epsilon a_1 b_1}{a_3} Y_1 X_2 \end{pmatrix}, \tag{3.25}$$

one obtains

$$DB_2(Y,X) = \begin{pmatrix} 0 & -\frac{\epsilon a_2 b_2}{a_1} X_3 & -\frac{\epsilon a_3 b_3}{a_1} X_2 \\ -\frac{\epsilon a_1 b_1}{a_2} X_3 & 0 & -\frac{\epsilon a_3 b_3}{a_2} X_1 \\ -\frac{\epsilon a_1 b_1}{a_3} X_2 & -\frac{\epsilon a_2 b_2}{a_3} X_1 & 0 \end{pmatrix}, \tag{3.26}$$

which leads to

$$\|DB_2(Y,X)\| \leq \left(\sum_{i,j=1}^3 \left\| [DB_2(Y,X)]_{i,j} \right\|^2 \right)^{1/2}$$
$$= \epsilon \left(\left[\left(\frac{a_2 b_2}{a_3}\right)^2 + \left(\frac{a_3 b_3}{a_2}\right)^2 \right] X_1^2 + \left[\left(\frac{a_1 b_1}{a_3}\right)^2 + \left(\frac{a_3 b_3}{a_1}\right)^2 \right] X_2^2 + \left[\left(\frac{a_1 b_1}{a_2}\right)^2 + \left(\frac{a_2 b_2}{a_1}\right)^2 \right] X_3^2 \right)^{1/2}. \tag{3.27}$$

Now, if the convex set $\mathscr{N}_\epsilon$ is contained within a ball of radius R centered at the origin, we obtain

$$\max_{(\mathbf{x},\mathbf{y})\in\mathscr{N}_\epsilon} \|DB_2(\mathbf{y},\mathbf{x})\| \leq \epsilon \left[\left(\frac{a_2 b_2}{a_3}\right)^2 + \left(\frac{a_3 b_3}{a_2}\right)^2 + \left(\frac{a_1 b_1}{a_3}\right)^2 + \left(\frac{a_3 b_3}{a_1}\right)^2 + \left(\frac{a_1 b_1}{a_2}\right)^2 + \left(\frac{a_2 b_2}{a_1}\right)^2 \right]^{1/2} R. \tag{3.28}$$

The estimate (3.19) on the Lipschitz constant follows now from (3.24). □

Incidentally, the upper bound in (3.17) splits the modeling error estimate, after division by ϵT, into the product of three terms, each of which taking its source in different aspects of the reduction problem: the L^2-average of the energy contained in the fast variable $\mathbf{x}_\epsilon$ (over $(t, t+\epsilon T)$), the nonlinear effects related to the size of the global attractor $\mathscr{A}_\epsilon$ (the radius R in (3.19)), and the parameterization defect of the manifold used in the reduction, here the BE manifold Φ_ϵ.

More generally, given two functions Ψ and Ψ' (mapping e.g. the vector space of the slow variables onto a space of fast variables), the parameterization defect is a natural non-dimensional number that allows us to compare objectively the corresponding manifolds in their ability to parameterize (possibly some of) the unresolved scales, here the fast variable $\mathbf{x}_\epsilon$ in the context of the rescaled PE model. Following [9,12], a manifold given as the graph of Ψ, is called a *parameterizing manifold (PM)*[9] if $Q(\Psi, T) < 1$.

Whereas an exact slaving corresponds to $Q \equiv 0$ (slow invariant manifold), the case $Q = 1$ corresponds to a limiting case in which $\Psi \equiv 0$, itself corresponding to a standard Galerkin approximation which differs from the QG Eq. (2.6); see Section 4.2 below. The error estimate (3.17) (that can be produced for any manifold function Ψ) shows that we are thus interested in manifolds for which $Q(\Psi, T, \epsilon) < 1$ and is actually as small as possible; see Section 4.1 below. In particular it excludes manifolds for which $Q(\Psi, T, \epsilon) > 1$ which would correspond to severe over- or under-parameterizations; see [12, Section 7.5] for an example in the stochastic context.

The goal is then to find a PM that comes with the smallest parameterization defect and that thus helps reduce the most the "unexplained" energy (associated here with $\mathbf{x}_\epsilon$) when the slow variables are mapped onto the manifold. This variational approach can even be made rigorous; see Theorem A.1 in Appendix A. Clearly, the residual of the energy left after mapping the slow rotational variables onto a PM (i.e. associated with $\mathbf{x}_\epsilon - \Phi_\epsilon(\mathbf{y}_\epsilon)$), even small, can turn out to be still determining for obtaining good modeling skill, thus involving the consideration of complementary parameterizations, possibly stochastic; see Section 4.3 below. At the same time, striking results can still be obtained by adopting the PM approach alone, as already demonstrated for the low-dimensional modeling of noise-induced large excursions arising in a stochastic Burgers equation [12, Chapters 6 and 7] or in the design of low-dimensional controllers for the optimal control of dissipative PDEs, for which rigorous error estimates clearly show the relevance of the notion of parameterization defect [9, Theorem 1 and Corrollary2]; see also the numerical results therein [9, Section 5.5].

In the context of this article, we show hereafter how the error estimates (3.17) and (3.19) allow us to predict outstanding modeling skills of the BE for $\epsilon < \epsilon_*$, while the numerical estimation of Q given in (3.16), ensures that the BE manifold is always a PM for the range of ϵ-values considered. The latter statement is shown in Fig. 6 for which the maximum defect of parameterization Q defined in (3.16) is strictly less than the unity, as computed here for $T = 80$ which corresponds to 10 days in the original physical time τ. It shows thus that the BE manifold is always a PM (for $\epsilon < 1.97$) over any 10-day window, a significant time-scale of the problem as pointed out in Section 2.3. For the estimation of the parameterization defect for (much) larger T we refer to Fig. 12 below.

To assess the relevance of the estimates derived in Proposition 3.1 regarding the modeling error, we computed an estimation of

$$\text{Mean Modeling Error} = \left\langle \frac{1}{\epsilon T} \left| \frac{\mathrm{d}\mathbf{y}_\epsilon}{\mathrm{d}t} - \left(L\mathbf{y}_\epsilon - \Phi_\epsilon(\mathbf{y}_\epsilon) \right) \right| \right.$$

[9] Variations about the precise definition of the parameterization defect can be used at this stage depending on the problem and the purpose but the general idea stays the same; compare with [9,12] and see also Section 4.1 below.

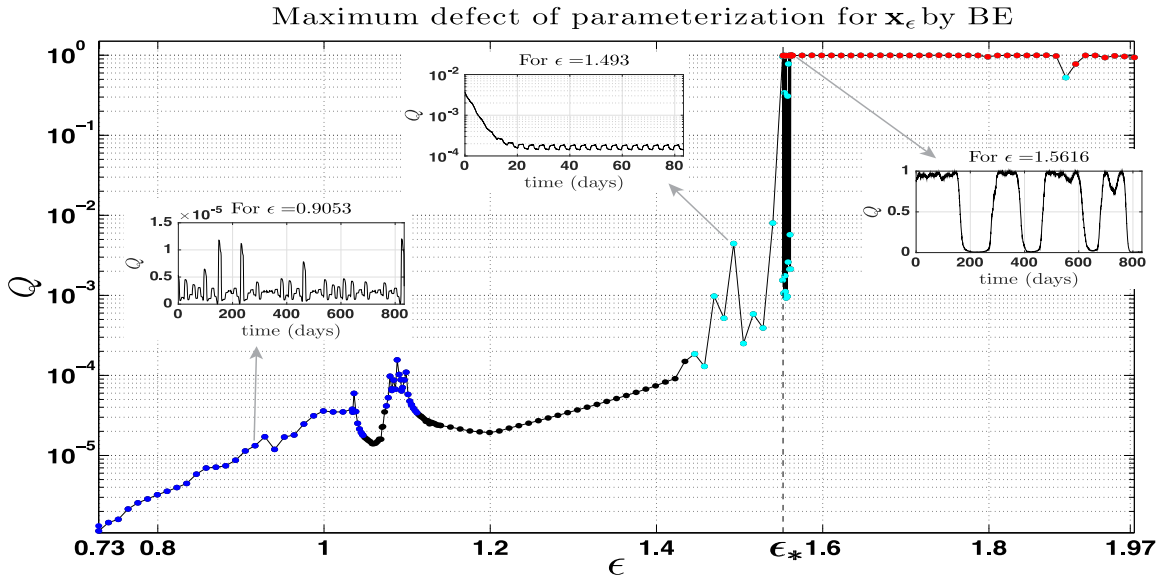

Fig. 6. Maximum defect of parameterization of the $\mathbf{x}_\epsilon$-variable by the BE manifold Φ_ϵ. Here T has been fixed to 80 in (3.16) for each ϵ, so that it corresponds to 10 days in the original time τ. Time-evolution of the parameterization defect "prior to taking the maximum" are displayed as inserts. The time-dependency of the parameterization defect in Regime IV (corresponding here to the red dots) reveals that it can fluctuate between values close to 1 or close to 0; the former being associated with an explosion of fast oscillations.

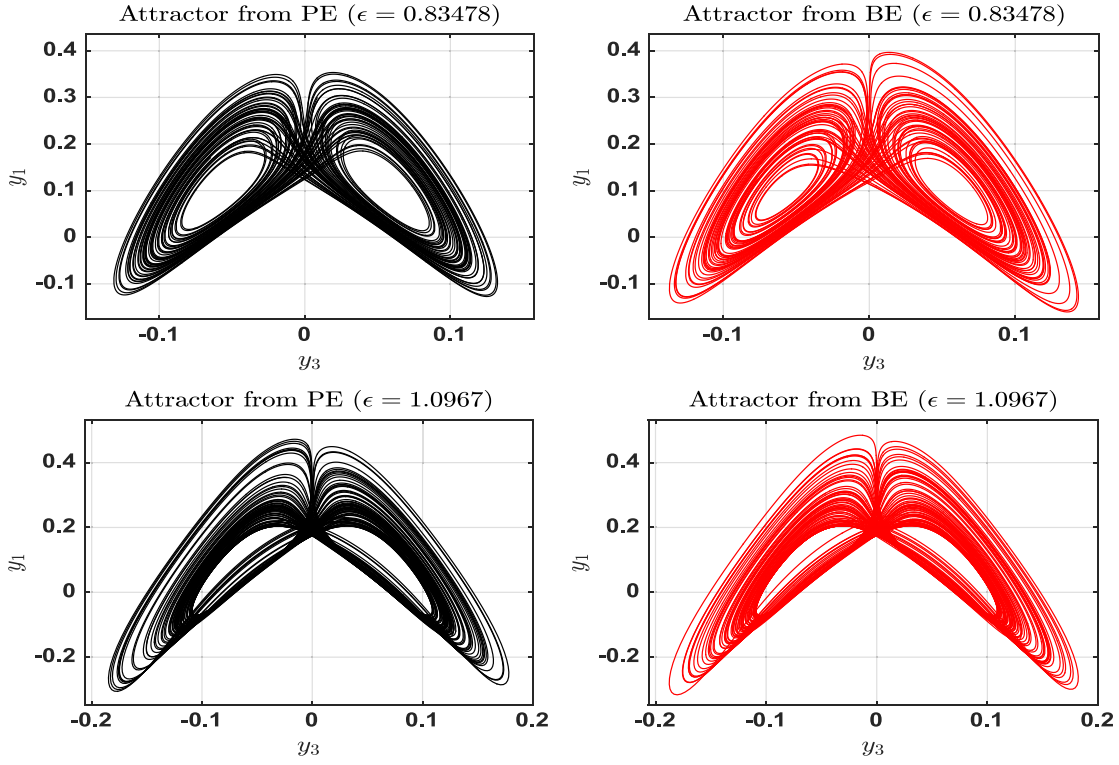

Fig. 7. Attractor comparison for $\epsilon = 0.83478$ and $\epsilon = 1.0967$. The (Y_1, Y_3)-projections of the attractor $\mathscr{A}_\epsilon$ associated with Eq. (2.5) (left panels) and their approximations obtained from the BE reduced model (3.10) (right panels), after rescaling using (3.11). Note the reminiscence with the famous Lorenz 1963 attractor [39] for those ϵ-values.

$$+ B_1\big(\mathbf{y}_\epsilon, \mathbf{y}_\epsilon\big) + B_2\big(\mathbf{y}_\epsilon, \Phi_\epsilon(\mathbf{y}_\epsilon)\big)\Big)\Big|^2_{L^2(t,t+\epsilon T)}\Big\rangle \tag{3.29}$$

by computing numerically the upper bounds in (3.17) and (3.19). In (3.29), $\langle f(t)\rangle$ denotes the average of f as t varies in $[t_1, t_2]$. Given the numerical setting of Section 2.3 we chose t_1 to be $2 \times 10^5 \delta t$, and t_2 to be $4.2 \times 10^6 \delta t - \epsilon T$. We discuss next the corresponding numerical results.

3.3. BE Modeling skills: numerical results

The metric (3.29) provides a measure of the BE skills to mimic, over a sliding 10-day window, the dynamics of the slow variable

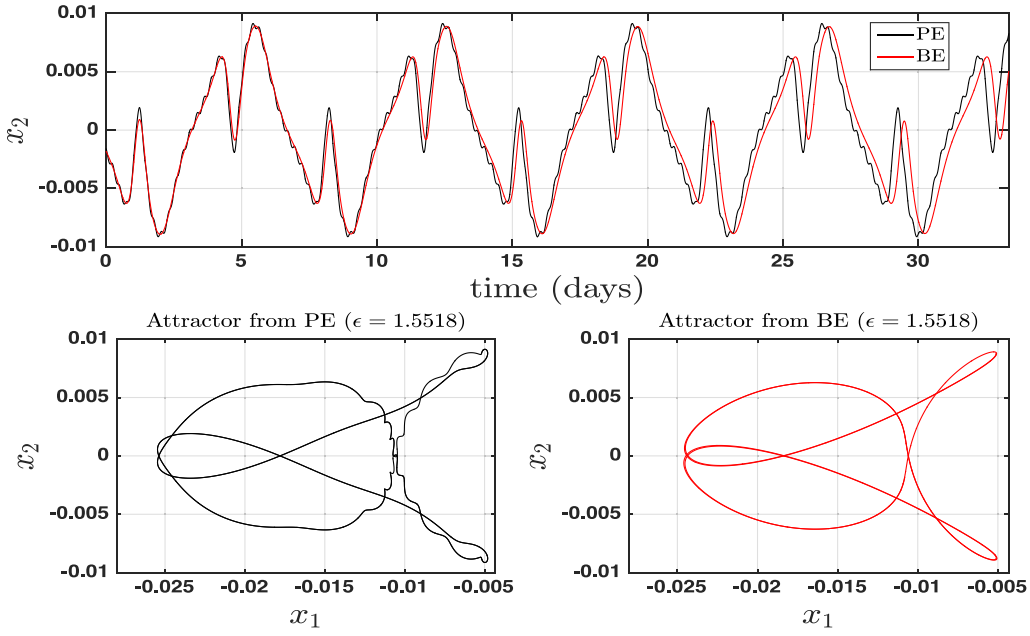

Fig. 8. Attractor comparison for $\epsilon = 1.5518$, "right below" ϵ_*. The (x_1, x_2)-projection of the attractor associated with Eq. (2.5) (lower-left panel) and its approximation obtained from the BE reduced model (3.10) (lower-right panel), after rescaling using (3.11). Here the choice of the variables x_1 and x_2 (compared to those used for Fig. 7) is motivated by a better readability of the "fuzziness" on these variables.

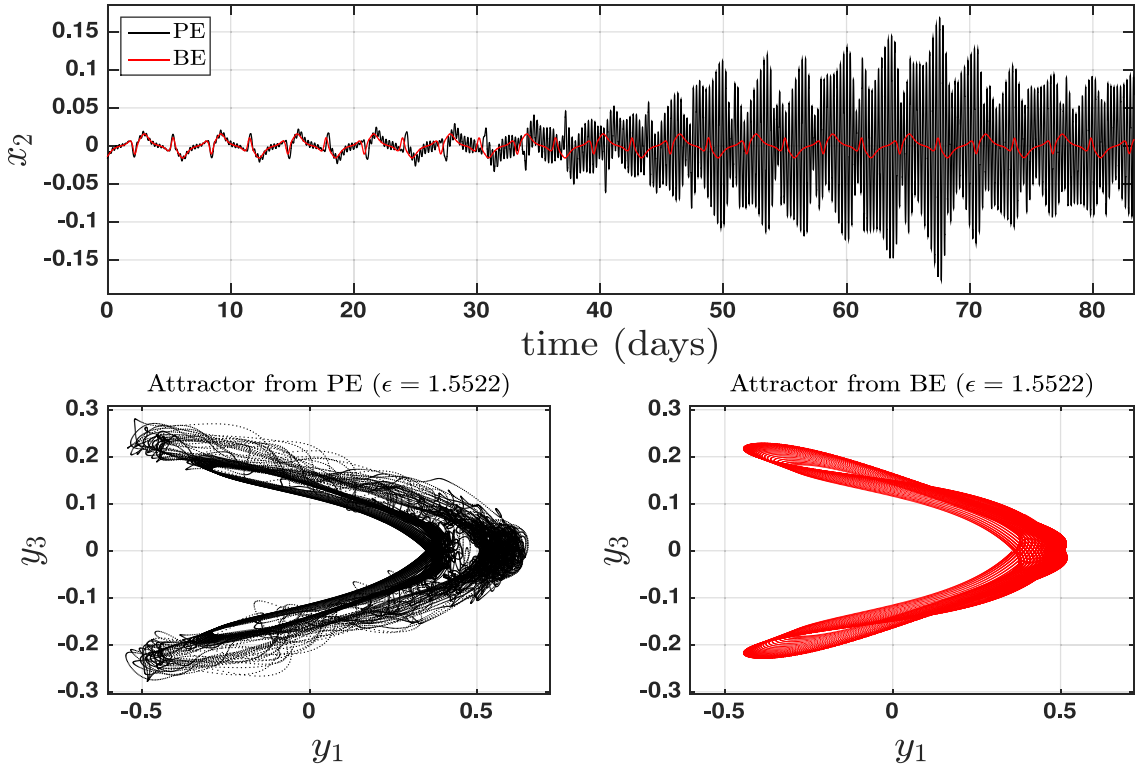

Fig. 9. Attractor comparison for $\epsilon = \epsilon_* = 1.5522$. The (Y_1, Y_3)-projection of the attractor associated with Eq. (2.5) (lower-left panel) and its approximation obtained from the BE reduced model (3.10) (lower-right panel), after rescaling using (3.11). Even in presence of energetic bursts of fast oscillations in the X_i-variables (here such a burst in X_2 is shown on the upper panel), the BE model is able to capture the coarse-grained topological features of the projected attractor onto the slow variables. This is an indication that the BE manifold provides a good approximation of the optimal PM given in (4.6) that averages out (optimally) the fast oscillations, by definition. This ability is even more remarkable given than the fraction of energy contained in the **x**-variable can reach within a burst up to 36.9 %, although subject to some initialization constraints for the BE; see Section 3.4.

Please cite this article as: M.D. Chekroun et al., The emergence of fast oscillations in a reduced primitive equation model and its implications for closure theories, Computers and Fluids (2016), http://dx.doi.org/10.1016/j.compfluid.2016.07.005

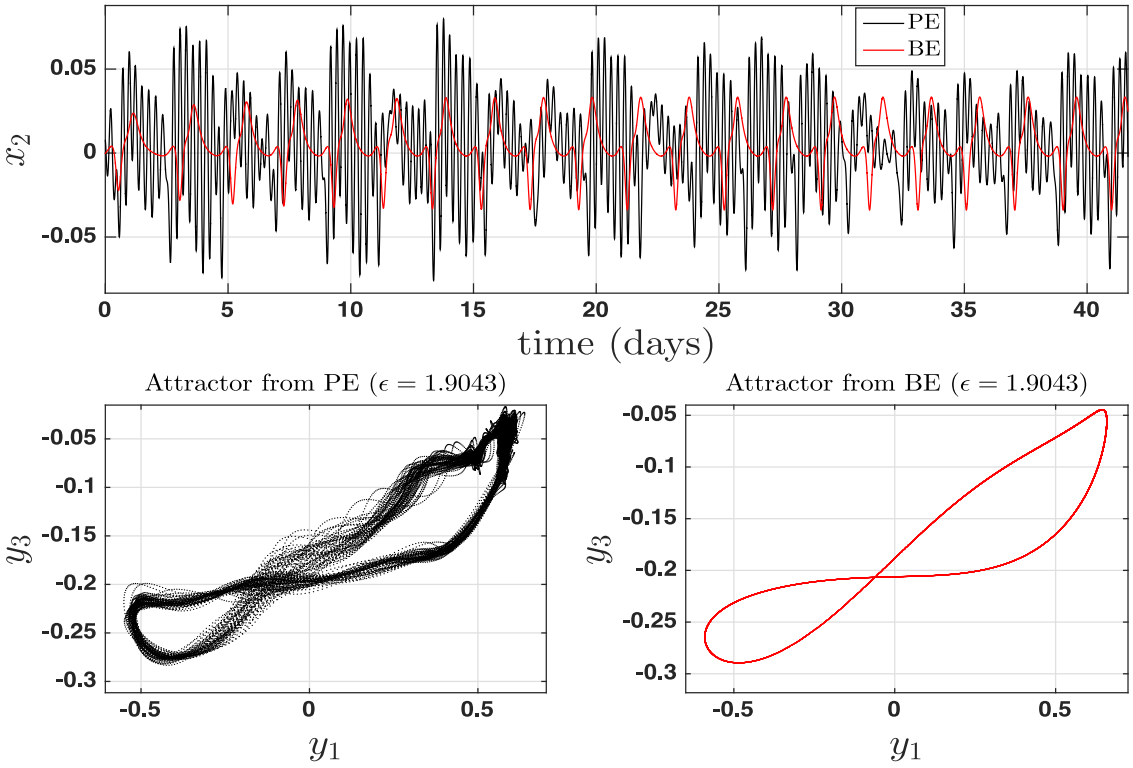

Fig. 10. Attractor comparison for $\epsilon = 1.9043$. As in Fig. 9 but here the fast oscillations in the X_i-variables (shown on the upper panel for X_2) are less energetic than in Fig. 9 but more pronounced than in Fig. 8. Here again, the BE model (3.10) is able to capture the coarse-grained topological features of the projected attractor onto the slow variables. This is an indication that the BE manifold provides a good approximation of the optimal PM given in (4.6) that, by definition, averages (optimally) out the fast oscillations.

Table 1
Mean modeling error as estimated from the upper bounds in (3.17) and (3.19) and averaged over the indicated ϵ-range.

ϵ-range	Mean modeling error (averaged)
$\epsilon \in [0.7280, 1.4342]$	4.1052×10^{-5}
$\epsilon \in [1.4459, 1.5518]$	7.337×10^{-1}
$\epsilon \in [\epsilon_*, 1.5618]$	38.5015

$\mathbf{y}_\epsilon$ as obtained from the rescaled PE. Table 1 shows that the estimates of Proposition 3.1 allows us to predict that the BE model performs outstandingly well for $\epsilon < 1.4342$. Essentially, these very good skills obtained from the BE model are obtained for ϵ-values corresponding to the blue and black dots shown in the previous figures; i.e. for Regimes I and II such as described in Section 2.3. For those regimes one can thus reasonably conjecture (conditioned to the numerical precision of our experiments) that a *slow invariant manifold exists*[10] and that the BE manifold constitutes a very good approximation of that slow manifold given the corresponding values of Q that are close to zero; see Fig. 6 and Table 2. The good modeling skills of the BE model in those regimes are shown by the reproduction of the main features of the strange PE attractor as shown in Fig. 7 for the (Y_1, Y_3)-projection and two arbitrary ϵ-values in Regime II.

Over the range $I_f = [1.4459, 1.5518]$ that roughly corresponds to the solutions (for $\epsilon < \epsilon_*$) that fall within Regime III discussed in Section 2.3, a change in the modeling skills is observed as witnessed by an increase of several order of magnitudes for both, the Q-values shown in Fig. 6 (cyan dots) and the mean modeling errors shown in Table 1. Such an increase of these numbers comes seemingly with a breakdown of exact slaving relationships, giving rise instead to a BE manifold that becomes a "fuzzy manifold," i.e. a manifold for which the attractor $\mathscr{A}_\epsilon$ lies within a thin neighborhood of that manifold. Fig. 8 illustrates such a behavior where fast gravity wave oscillations — of weak energy compared to the dominant low-frequency oscillations corresponding to the Rossby waves — develop within a thin layer around the BE manifold (red curve).

The resulting BE attractor for $\epsilon = 1.5518$ — located right below ϵ_* according to our ϵ-mesh resolution — is smoother than the PE attractor but still captures the main topological features of PE attractor's global shape as shown by comparing the lower-left panel with the lower-right panel of Fig. 8. This scenario of approximation is somewhat consistent with the exponential smallness bounds obtained in [57,58] for the hydrostatic (non-truncated) primitive equations with viscous terms, and indicates that such smallness bounds (although not necessarily exponential) are expected to hold for the rescaled (truncated) PE model (2.5), over the small ϵ-range I_f. As it will be discussed in Section 4 below, approaches such as [57,58], relying on ideas rooted in the theory of *approximate inertial manifolds (AIMs)* [24,53,55], needs to be completed by other approaches for both, the rigorous analysis and the numerical treatment of the closure problem beyond ϵ_*, where the emergence of explosive bursts of fast oscillations takes place; see Section 4.3. To nurture this discussion within the scope of this article, we report hereafter about some examples of modeling skills that can be obtained by the BE model in the presence of such bursts.

Two values of ϵ are selected here for that purpose. The value $\epsilon = \epsilon_* \approx 1.5522$ for which explosive bursts occur (see Figs. 3 and 4) and the value $\epsilon = 1.9043$ for which the bursts of fast oscillations are much less energetic; compare upper panels of Figs. 9 and

[10] In consistency with the slow manifold existence result of [35] for small dissipation and forcing, although [35] does not provide explicit thresholding estimates regarding the breakdown of slaving principle.

Table 2
Mean modeling error as estimated from the upper bound in (3.17) along with their constitutive ingredients.

ϵ	Upper bound in (3.19)	Q	$\left\langle \frac{1}{\epsilon T} \lvert \mathbf{x}_\epsilon \rvert^2_{L^2(t,t+\epsilon T)} \right\rangle$	Mean modeling error
$\epsilon = 1.9043$	15.1400	7.773×10^{-1}	3.96×10^{-1}	70.93
$\epsilon = 1.7398$	20.8987	9.991×10^{-1}	2.3458	1026
$\epsilon = \epsilon_*$	14.118	9.9848×10^{-1}	0.2174	42.89
$\epsilon = 1.5518$	7.3965	1.5×10^{-3}	5.73×10^{-2}	4.9×10^{-3}
$\epsilon = 1.0967$	6.0362	8.78×10^{-5}	4.96×10^{-2}	1.63×10^{-4}
$\epsilon = 0.8348$	3.1865	4.47×10^{-6}	5.09×10^{-2}	2.53×10^{-6}
$\epsilon = 0.7408$	2.5005	1.45×10^{-6}	5.11×10^{-2}	5.38×10^{-7}

10. The latter value lies within the ϵ-range (above $\epsilon = 1.8$) where a drop can be observed in the metrics shown in Fig. 5 about the energy, and also in the maximum defect of parameterization[11] Q; see Fig. 6. Compare to the fuzzy-manifold case just discussed above, error estimates of Proposition 3.1 predict here an increase of the Mean Modeling Error to 42.89 and 70.93, respectively. These increases correspond to an actual deterioration of the BE modeling skills that are visible by comparing the PE and BE attractors; comparison that shows at the same time a certain ability in reproducing the coarse-grained topological features of the PE attractor as projected on the slow variables; see Fig. 10.

This ability in reproducing the coarse-grained topological features of the PE attractor even in presence of bursts of fast oscillations is somewhat more striking for $\epsilon = \epsilon_*$, a case for which the fraction of energy contained in the **x**-variable can reach up to 36.9 % within a burst episode. Such averaging skills of the BE will be clarified within the framework of the slow conditional expectation of Section 4. We discuss hereafter some initialization constraints to be however taken into account so that the BE operates properly in presence of bursts.

3.4. BE initialization

While the ability of the BE to mimic the PE long-term dynamics is mostly insensitive to the choice of the BE initial data for $\epsilon < \epsilon_*$, it has been numerically observed that starting at $\epsilon \approx \epsilon_\# = 1.5165$ that lies within the fuzzy-manifold regime (i.e. the cyan zone of the previous plots), the BE — when initialized with the perturbation of the Hadley fixed point for the BE used in [27, Eqns. (34)] — fails in reproducing the global topological shape of the PE attractor. This failure cannot be predicted by the mean modeling error that is by definition a discrepancy measure of the BE manifold along the true solution $\mathbf{y}_\epsilon$ generated by the rescaled PE, and which thus does not take into account how the (long-term) dynamics of the BE model may depend on its initialization.

Nevertheless, this initialization issue turns out to be rectifiable even beyond ϵ_*, in presence of explosive fast oscillations. It consists of initializing the BE based on the simulated rescaled PE solution at time instances for which the fast oscillations are not energetic. Such a rectification is operationally effective and has been used to produce the results of Figs. 8, 9, and 10. More precisely, the BE initialization used for these figures are taken to be $\epsilon Y(n\delta t)$ with $Y(n\delta t)$ denoting the Y-component of the simulated rescaled PE solution at $t = n\delta t$, where we have taken $n = 10^6$ for $\epsilon = 1.5518$, $n = 7.5 \times 10^5$ for $\epsilon = \epsilon^* = 1.5522$, $n = 1.2 \times 10^6$ for $\epsilon = 1.9043$. Finally, it has been observed that the BE when initialized within a burst, can still provide a good reproduction of the global shape of the PE attractor, although this observation requires more understanding. Noteworthy is the case $\epsilon = 1.7398$ of Fig. 11 where the failure of capturing the lobe dynamics is not related to the BE initialization but due to other reasons that will be clarified in Section 4.3.

[11] To be more precise it corresponds to the red dot located next to the right of the isolated cyan dot whose ϵ-value is > 1.8.

4. Parameterizing manifolds and the slow conditional expectation

The partial failure of the BE model pointed out in Fig. 11 illustrates that a PM alone may turn out to be insufficient for obtenting a satisfactory closure model of the slow variables, and may require correction terms. In this section we delineate a theoretical framework that helps understand the nature of these corrections terms, especially when $\epsilon > \epsilon_*$. The actual design of such correction terms in the context of (2.5) will be reported elsewhere. Our approach relies on the ergodic theory of chaos which provides a theory of *long-term statistical properties* of chaotic (and dissipative) dynamical systems [14,19,70], the Mori–Zwanzig approach to the closure problem from statistical mechanics [7,33], and the parameterizing manifold approach [9,12]. The framework allows us also to provide new insights to the parameterizing problem of the fast variables in terms of slaving relationships and other notion of "fuzzy manifold." It is shown indeed that a theoretical limit to this problem can be formulated in terms of a variational principle related to the notion of parameterizing defect discussed above (see Theorem A.1), and a notion of slow conditional expectation such as explained below.

4.1. Parameterizing manifolds and slow conditional expectations

Let us first rewrite Eq. (2.5) into the following abstract form

$$\dot{u} = \mathbf{R}_\epsilon(u), \quad u = (\mathbf{x}_\epsilon, \mathbf{y}_\epsilon, \mathbf{z}_\epsilon). \tag{4.1}$$

Here u lives in $\mathscr{H} = \mathbb{R}^9$ and is decomposed as

$$\mathscr{H} = \mathscr{H}_{\mathfrak{f}_1} \times \mathscr{H}_{\mathfrak{s}} \times \mathscr{H}_{\mathfrak{f}_2}, \tag{4.2}$$

where $\mathbf{x}_\epsilon$ lives in $\mathscr{H}_{\mathfrak{f}_1}$, $\mathbf{y}_\epsilon$ in $\mathscr{H}_{\mathfrak{s}}$ and $\mathbf{z}_\epsilon$ in $\mathscr{H}_{\mathfrak{f}_2}$.

We assume that (4.1) possesses an invariant measure μ that is *physically relevant* [5, Sec. 5.7] in the sense that for any Lebesgue-positive set $\mathfrak{B}$ in the *basin of attraction* $\mathfrak{B}(\mu)$ of μ, and for any (continuous) observable $\varphi : \mathscr{H} \to \mathbb{R}$, the following ergodic property holds

$$\lim_{T\to\infty} \frac{1}{T} \int_0^T \varphi(S_\epsilon^t u_0)\, \mathrm{d}t = \int_{\mathscr{H}} \varphi(u) \mathrm{d}\mu(u), \quad u_0 \in \mathfrak{B}, \tag{4.3}$$

where $(S_\epsilon^t)_{t\in\mathbb{R}}$ denotes the solution operator associated with (4.1), i.e. its (phase) flow or one-parameter group of transformations in the language of dynamical system theory [1]. A physical measure is thus associated with a stronger but more natural notion of ergodicity than with Birkhoff ergodic theorem which states (4.3) but only for μ-almost all initial data. Indeed, when a physical measure exists, it says essentially that the long-term statistics estimated from *Lebesgue-almost* any arbitrary time series generated by the system, are not sensitive to its initial state provided that the latter lives within $\mathfrak{B}(\mu)$ [5]. In that sense, the statistical equilibrium μ is typical and describes the long-term statistics of almost all trajectories. This assumption is often referred as the *chaotic hypothesis* [25].

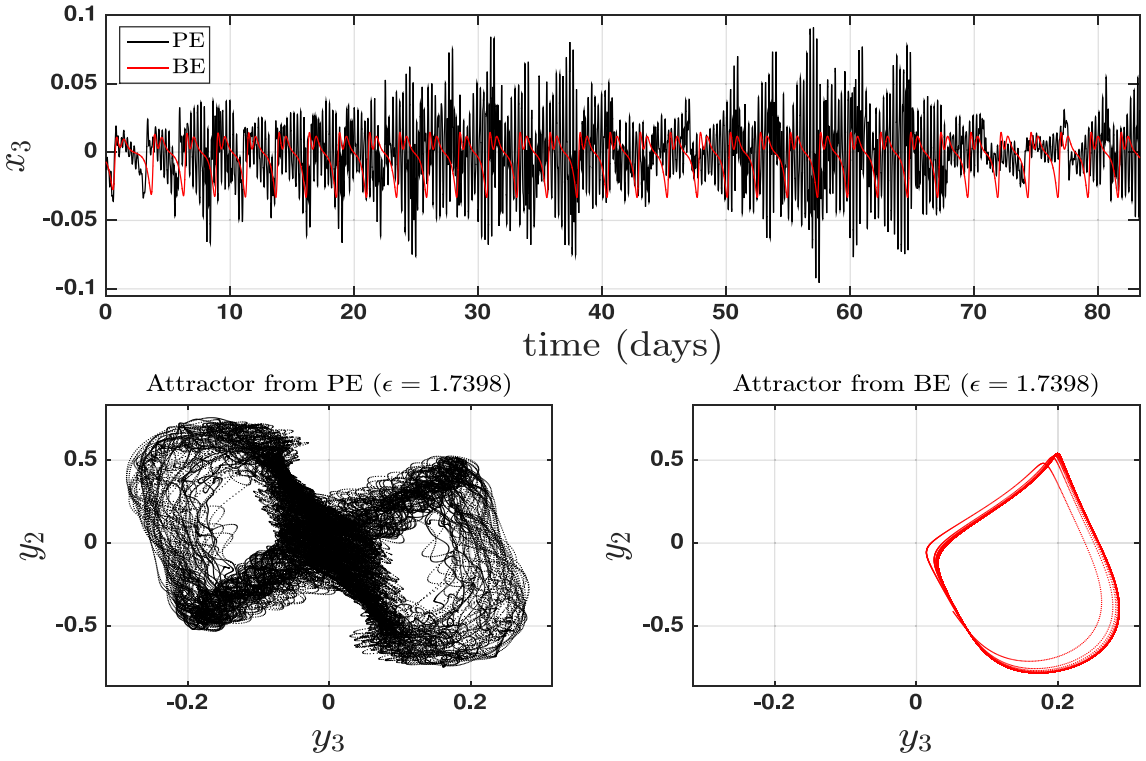

Fig. 11. Attractor comparison for $\epsilon = 1.7398$. As in Fig. 9 but for the (Y_2, Y_3)-projection. As defined in (4.6), the optimal PM is aimed to average out optimally the fast oscillations. Here, only one lobe of the attractor is smoothed by the BE which shows a partial success in approximating the optimal PM (for one lobe), but at the same time fails to reproduce the relevant connecting orbits.

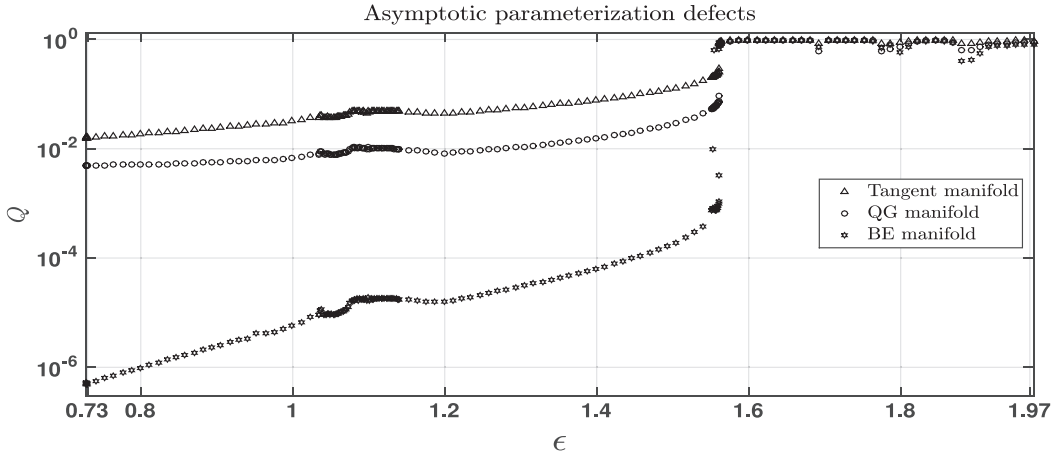

Fig. 12. Asymptotic parameterizing defects for the BE, the QG, and the tangent manifolds.

Given the projection Π_s onto the vector space of slow variables $\mathscr{H}_s$, we define the following *slow conditional expectation* of the vector field in Eq. (3.20) (corresponding to the RHS of the Y-equations in Eq. (2.5)) associated with Π_s and the statistical equilibrium μ

$$\overline{\Pi_s \mathbf{R}}(\mathbf{y}) := \int_{\mathbf{x}\in\mathscr{H}_{f_1}} \Big[L\mathbf{y} - \mathbf{x} + B_1(\mathbf{y},\mathbf{y}) + B_2(\mathbf{y},\mathbf{x})\Big]\, \mathrm{d}\mu^1_{\mathbf{y}}(\mathbf{x}),$$
$$= L\mathbf{y} + B_1(\mathbf{y},\mathbf{y}) + \int_{\mathbf{x}\in\mathscr{H}_{f_1}} \Big[B_2(\mathbf{y},\mathbf{x}) - \mathbf{x}\Big]\, \mathrm{d}\mu^1_{\mathbf{y}}(\mathbf{x}), \quad (4.4)$$

in which we have dropped the ϵ-subscript to avoid superfluous notations. Here $\mu^1_{\mathbf{y}}$ denotes the disintegrated probability distribution on the vector space $\mathscr{H}_{f_1}$ corresponding to the fast variable $\mathbf{x}$ and conditioned on the slow variable $\mathbf{y}$; see [13, Supporting Information]. The probability measure $\mu^1_{\mathbf{y}}$ can be rigorously defined, for any function f with the nice integrability condition [16, p. 78], through the relation

$$\int_{\mathscr{H}} f(\mathbf{x},\mathbf{y})\, \mathrm{d}\mu(\mathbf{x},\mathbf{y},\mathbf{z}) = \int_{\mathscr{H}_s} \Big(\int_{\mathbf{x}\in\mathscr{H}_{f_1}} f(\mathbf{x},\mathbf{y})\, \mathrm{d}\mu^1_{\mathbf{y}}(\mathbf{x}) \Big)\, \mathrm{d}\mathfrak{m}(\mathbf{y}), \quad (4.5)$$

where $\mathfrak{m}$ is the *push-forward* of the measure μ by Π_s on the vector space of slow variables, i.e. $\mathfrak{m}(E) = \mu(\Pi_s^{-1}(E))$, for any Borel set E of $\mathscr{H}_s$, denoted hereafter $\mathfrak{m} = \Pi_s * \mu$. More intuitively, the probability measure $\mu^1_{\mathbf{y}}$ can be interpreted as providing the statistics of the fast unobserved variables $\mathbf{x}$ when the slow variable is in an ob-

served state[12] $\mathbf{y}$ [13, Supporting Information]; fast variables whose effects need to be appropriately parameterized to model the dynamics of the slow (observed) variables [13,33].

As a conditional expectation, the vector field $\overline{\Pi_s \mathbf{R}}$ in (4.4) provides the vector field of $\mathscr{H}_s$ (depending on $\mathbf{y}$ only) that best approximates the vector field (depending on $\mathbf{x}$) given by $\Pi_s\mathbf{R} : u \mapsto L\mathbf{y} - \mathbf{x} + B_1(\mathbf{y},\mathbf{y}) + B_2(\mathbf{y},\mathbf{x})$; where u is as defined in (4.1). It provides thus the best approximation of $\Pi_s\mathbf{R}$ for which the fast variables $\mathbf{x}$ are averaged out, supporting thus the terminology of slow conditional expectation.

If one defines now a mapping $h : \mathscr{H}_s \to \mathscr{H}_{f_1}$ by

$$h(\mathbf{y}) = \int_{\mathscr{H}_{f_1}} \mathbf{x}\, \mathrm{d}\mu^1_{\mathbf{y}}(\mathbf{x}), \quad \mathbf{y} \in \Pi_s \mathscr{A}, \tag{4.6}$$

then a simple calculation shows that

$$\overline{\Pi_s \mathbf{R}}(\mathbf{y}) = L\mathbf{y} + B_1(\mathbf{y},\mathbf{y}) + B_2(\mathbf{y}, h(\mathbf{y})) - h(\mathbf{y}). \tag{4.7}$$

Note that the support of the probability measure $\mu^1_{\mathbf{y}}$ in (4.6) is actually contained in the compact set $\Pi_{f_1}\mathscr{A}$ since the support of the statistical equilibrium μ satisfying (4.3) is contained in the global attractor $\mathscr{A}$ as for any invariant measure (e.g. [6, Lemma 5.1]), and the global attractor $\mathscr{A}$ is compact [55, Definiton 1.3.].

As shown in Theorem A.1 (see Appendix A), the parameterization h minimizes furthermore over all the possible square-integrable mappings[13] from $\mathscr{H}_s$ to $\mathscr{H}_{f_1}$, the following *parameterizing defect functional*:

$$J(\Psi) = \lim_{T\to\infty} \frac{1}{T} \int_0^T \left\| \mathbf{x}(t) - \Psi(\mathbf{y}(t)) \right\|^2 \mathrm{d}t, \ (\mathbf{x}(t),\mathbf{y}(t),\mathbf{z}(t)) \in \mathscr{A}. \tag{4.8}$$

Since $J(0) = \lim_{T\to\infty} \frac{1}{T}\int_0^T \left\|\mathbf{x}(t)\right\|^2 \mathrm{d}t$, one has necessarily that $J(h) \leq J(0)$. It is thus natural to introduce the notion of *asymptotic parameterizing manifold* by requiring that h satisfies

$$\int_0^T \left\| \mathbf{x}(t) - h(\mathbf{y}(t)) \right\|^2 \mathrm{d}t < \int_0^T \left\| \mathbf{x}(t) \right\|^2 \mathrm{d}t, \quad \text{for all } T \text{ sufficiently large.} \tag{4.9}$$

Taking the limit as $T \to \infty$ of the ratio of the LHS with the RHS, one obtains an asymptotic parameterizing defect Q that in practice we will still denote by Q once T has been fixed to a sufficiently large value. It appears thus that when $Q < 1$, the manifold function h (given by (4.6)) provides the best (asymptotic) parameterizing manifold of the fast dynamics on the attractor $\mathscr{A}$, given the slow-variable projection Π_s.

The analytical or numerical determination of the optimal PM, h, by using (4.6) is however a non-trivial task to reach in practice since it relies implicitly on the knowledge of $\mu^1_{\mathbf{y}}$, as $\mathbf{y}$ varies over the attractor; probability measures that require either intensive or intractable computations for forced-dissipative chaotic systems. The backward-forward approach introduced in [9,12][14] provides an efficient alternative and a general approach for the derivation of analytical formulas of PMs of various parameterization defects and order, although *a priori estimates* to the distance to the optimal parameterizing manifold are not yet available within this framework.

In the context of this article, the computation of the maximum parameterizing defect for Eq. (2.5) (over a sliding 10-day window; see Fig. 6) strongly indicates that for $\epsilon < \epsilon_*$, the BE manifold provides an excellent approximation of the optimal parameterizing manifold h (defined in (4.6)) and thus of the slow conditional expectation (4.4). This is further discussed in Section 4.2 below. The numerical results of Section 3.3 gathered in Tables 1 and 2 on one hand, and in Figs. 7 and 8, on the other, show thus that for $\epsilon < \epsilon_*$, a good approximation of the slow conditional expectation is sufficient for the reproduction of the PE dynamics in terms of the slow variables, solely.

It will be (briefly) discussed below in Section 4.3 how non-Markovian and stochastic corrective terms to the BE manifold become actually crucial to pursue such modeling skills for $\epsilon \geq \epsilon_*$, when the explosion of fast oscillations take place. In the meantime, we analyze in the next section whether the nonlinear effects brought in Eq. (3.10) by the BE manifold are really needed for obtaining the good modeling skill shown in Section 3.3 for $\epsilon < \epsilon_*$, i.e. when both the energy and the fraction of energy contained in the fast variable $\mathbf{x}$ are small; see Fig. 5. Indeed the latter energy balance, could let to believe that simpler parameterizations than the BE would be sufficient to reproduce the dynamics. This is actually not so simple, and as shown below, even a small fraction of energy contained in the fast variables requires an appropriate parameterization to get the slow dynamics right.

4.2. Comparison with other natural manifolds

A first natural manifold to compare with the BE manifold, is its tangent linear approximation. In this way, we arrive at a quadratic version of Eq. (3.10) in which the Φ-terms are replaced by linear ones, and that can serve thus as a reference for analyzing (implicitly) any usefulness of other nonlinear terms than quadratic that the BE manifold would brought in Eq. (3.10), for modeling purposes. Furthermore, this quadratic version allows for further comparison with the Quasigeostrophic (QG) manifold that can be derived for $\epsilon = 0$ and is associated with the famous quadratic Lorenz system [39]; see below.

4.2.1. The tangent manifold to BE

While the BE manifold Φ given by (3.9) is given implicitly, its tangent approximation at $\mathbf{y} = \mathbf{0}$ can be obtained analytically. The derivation is performed below for the sake of clarity.

First note that $G(\mathbf{0}) = \mathbf{0}$. By using Eqs. (3.7) and (3.8), we get by setting $\mathbf{x} = \mathbf{y} = \mathbf{z} = 0$ therein

$$M(\mathbf{0}, G(\mathbf{0})) = \begin{pmatrix} 1+g_0a_1 & 0 & 0 \\ 0 & 1+g_0a_2 & b_1h_1 \\ 0 & b_1h_1 & 1+g_0a_3 \end{pmatrix},$$
$$\begin{pmatrix} d_{1,2,3}(\mathbf{0}, G(\mathbf{0})) \\ d_{2,3,1}(\mathbf{0}, G(\mathbf{0})) \\ d_{3,1,2}(\mathbf{0}, G(\mathbf{0})) \end{pmatrix} = -\begin{pmatrix} F_1 \\ 0 \\ 0 \end{pmatrix}, \tag{4.10}$$

where we have used $h_2 = h_3 = F_2 = F_3 = 0$ as given in (2.3). Using (4.10) in (3.9), we get

$$\Phi(\mathbf{0}) = \left(-\frac{F_1}{1+g_0a_1}, 0, 0 \right)^T, \tag{4.11}$$

under the assumption that

$$(1+g_0a_2)(1+g_0a_3) - (b_1h_1)^2 \neq 0, \tag{4.12}$$

which is always true for the parameter values used in this article; see again (2.3). Condition (4.12) is in any case, a necessary condition to the existence of Φ given by (3.9).

The Jacobian matrix of Φ at $\mathbf{y} = \mathbf{0}$ can be obtained by first using $\mathbf{z} = G(\mathbf{y})$ in Eq. (3.7), and then differentiating both sides of (3.7) with respect to y_i for $i = 1, 2, 3$ and setting $\mathbf{y} = \mathbf{0}$. This calculation leads to a linear system with a matrix RHS, to be solved

[12] Here the observation of the system is assumed to be partial as resulting from application of the projection Π_s.

[13] More precisely, the mappings that belong to the vector space of $\mathscr{H}_{f_1}$-valued square-integrable functions Ψ with respect to $\mathfrak{m} = \Pi_s * \mu$, i.e. in the Hilbert space $L^2_{\mathfrak{m}}(\mathscr{H}_s; \mathscr{H}_{f_1})$.

[14] And rooted in the approximation theory of invariant manifolds [11].

in order to find the entries of the Jacobian matrix of Φ at $\mathbf{y}=\mathbf{0}$. This system can be compactly written as follows

$$M(\mathbf{0}, G(\mathbf{0}))D\Phi(\mathbf{0}) = \begin{pmatrix} 0 & 0 & 0 \\ 0 & 0 & l_2 \\ 0 & l_1 & 0 \end{pmatrix}. \tag{4.13}$$

Here $M(\mathbf{0}, G(\mathbf{0}))$ is given by (4.10), and $D_{\mathbf{y}}\Phi(\mathbf{0})$ denotes

$$D_{\mathbf{y}}\Phi(\mathbf{0}) := \begin{pmatrix} \frac{\partial\Phi_1}{\partial y_1}(\mathbf{0}) & \frac{\partial\Phi_1}{\partial y_2}(\mathbf{0}) & \frac{\partial\Phi_1}{\partial y_3}(\mathbf{0}) \\ \frac{\partial\Phi_2}{\partial y_1}(\mathbf{0}) & \frac{\partial\Phi_2}{\partial y_2}(\mathbf{0}) & \frac{\partial\Phi_2}{\partial y_3}(\mathbf{0}) \\ \frac{\partial\Phi_3}{\partial y_1}(\mathbf{0}) & \frac{\partial\Phi_3}{\partial y_2}(\mathbf{0}) & \frac{\partial\Phi_3}{\partial y_3}(\mathbf{0}) \end{pmatrix} \tag{4.14}$$

and

$$\begin{aligned} l_1 &= -ch_1 - \frac{(2c^2 - a_2b_2 + a_3b_2)F_1}{a_3(1+g_0a_1)}, \\ l_2 &= ch_1 - \frac{(2c^2 - a_3b_3 + a_2b_3)F_1}{a_2(1+g_0a_1)}. \end{aligned} \tag{4.15}$$

The tangent approximation to the BE manifold at $(\mathbf{0}, \Phi(\mathbf{0}))$ is then given by:

$$\Psi(\mathbf{y}) = \Phi(\mathbf{0}) + D_{\mathbf{y}}\Phi(\mathbf{0})\mathbf{y}, \tag{4.16}$$

and it takes the following explicit form:

$$\Psi(\mathbf{y}) = \begin{pmatrix} -\frac{F_1}{1+g_0a_1} \\ 0 \\ 0 \end{pmatrix} + \begin{pmatrix} 0 & 0 & 0 \\ 0 & \alpha_1 & \alpha_2 \\ 0 & \beta_1 & \beta_2 \end{pmatrix}\mathbf{y}, \tag{4.17}$$

where

$$\begin{aligned} \alpha_1 &= -\frac{b_1h_1l_1}{(1+g_0a_2)(1+g_0a_3) - (b_1h_1)^2}, \\ \beta_1 &= \frac{(1+g_0a_2)l_1}{(1+g_0a_2)(1+g_0a_3) - (b_1h_1)^2}, \\ \alpha_2 &= \frac{(1+g_0a_3)l_2}{(1+g_0a_2)(1+g_0a_3) - (b_1h_1)^2}, \\ \beta_2 &= -\frac{b_1h_1l_2}{(1+g_0a_2)(1+g_0a_3) - (b_1h_1)^2}, \end{aligned} \tag{4.18}$$

Replacing Φ in (3.10) by Ψ just derived, one obtains the following reduced system

$$\begin{aligned} a_i\frac{dy_i}{d\tau} &= -a_kb_k\Psi_j(\mathbf{y})y_k - a_jb_jy_j\Psi_k(\mathbf{y}) \\ &\quad + c(a_k - a_j)y_jy_k - a_i\Psi_i(\mathbf{y}) - \nu_0a_i^2y_i, \end{aligned} \tag{4.19}$$

that we will refer hereafter as the *tangent approximation to BE*. Intuitively, this tangent approximation should score well in regimes where when both the energy and the fraction of energy contained in the fast variable $\mathbf{x}$ are small i.e. for $\epsilon < \epsilon_*$; see Fig. 5. In Section 4.2.3 below, we show that this intuition, although confirmed to a certain extent, needs to be rightly nuanced.

4.2.2. The parameterizing manifold associated with the QG model

Recall that the QG model as given in [40, Eq. (43)] (and written above as (2.6) for the rescaled PE) can be derived from the PE (2.1) by removing from Eq. (2.1a) the term $\frac{d\mathbf{x}}{d\tau}$ and all the terms involving $\mathbf{x}$ as well as by removing from Eqs. (2.1b)–(2.1c) all the nonlinear terms and topographic terms containing $\mathbf{x}$. This operation leads to following set of equations

$$y_i = z_i, \tag{4.20a}$$

$$a_i\frac{dy_i}{d\tau} = c(a_k - a_j)y_jy_k - a_ix_i - \nu_0a_i^2y_i, \tag{4.20b}$$

$$\frac{dz_i}{d\tau} = cy_j(z_k - h_k) - c(z_j - h_j)y_k + g_0a_ix_i - \kappa_0a_iz_i + F_i. \tag{4.20c}$$

The QG model is then obtained by multiplying (4.20b) by g_0 and then adding to (4.20c), where the $\mathbf{z}$-variable is eliminated using (4.20a). Note that an explicit parameterization of $\mathbf{x}$ in terms of $\mathbf{y}$ can be obtained by multiplying (4.20c) by $-a_i$ and then adding to (4.20b) and solving for $\mathbf{x}$, where the $\mathbf{z}$-variable is eliminated again by using (4.20a). This way, we obtain

$$\begin{aligned} x_i = \frac{1}{a_i + g_0a_i^2}\Big(&a_i^2(\kappa_0 - \nu_0)y_i + ca_ih_ky_j - ca_ih_jy_k \\ &+ c(a_k - a_j)y_jy_k - a_iF_i\Big). \end{aligned} \tag{4.21}$$

Under the conditions $a_1 = a_2$, $\kappa_0 = \nu_0$ and $h_2 = h_3 = F_2 = F_3 = 0$ as given in (2.3), this parameterization can be further reduced to:

$$\begin{aligned} x_1 &= -\frac{F_1}{1+g_0a_1} + \frac{c(a_3 - a_2)}{a_1(1+g_0a_1)}y_2y_3, \\ x_2 &= \frac{1}{a_2(1+g_0a_2)}\Big(ca_2h_1y_3 + c(a_1 - a_3)y_1y_3\Big), \\ x_3 &= -\frac{ch_1y_2}{1+g_0a_3}. \end{aligned} \tag{4.22}$$

We will refer hereafter to this parameterization as the *QG manifold*.

4.2.3. Comparison

Given a manifold function $\varphi : \mathscr{H}_{\mathfrak{s}} \to \mathscr{H}_{\mathfrak{f}_1}$, we computed, as ϵ is varying, its parameterization defect Q given by:

$$Q(\varphi, T, \epsilon) := \frac{\int_0^{\epsilon T} \left\|\mathbf{x}_\epsilon(t) - \varphi(\mathbf{y}_\epsilon(t))\right\|^2 dt}{\int_0^{\epsilon T} \|\mathbf{x}_\epsilon(t)\|^2 dt}, \tag{4.23}$$

where ϵT corresponds to 4×10^6 data points; see Section 2.3.

The results presented in Fig. 12 clearly show a ranking of the parameterization defects as given by (4.23) for $\epsilon < \epsilon_*$. The best score is achieved by the BE, while the QG and tangent manifolds have similar parameterization defects with a slight advantage for the QG manifold. For $\epsilon \geq \epsilon_*$, the ranking is blurred within a tiny neighborhood close to 1 from below, showing at least that the QG and the tangent manifolds are PMs for the range of ϵ-values considered here.

A closer look at the dynamical behavior associated with the QG Eq. (2.6), on one hand, and Eq. (3.10) in which the tangent manifold Ψ replaces the BE manifold Φ, on the other, reveals interesting distinctions. For instance while a reduced model based on the tangent manifold is able to reproduce for $\epsilon = 0.83478$ the attractor global shape of the ((Y_1, Y_3)-projection of the) PE attractor (compare left panel of Fig. 13 with the upper-left panel of Fig. 7), the QG attractor reduces to a steady state (not shown).[15] For $\epsilon = 1.0967$ it is now the QG attractor that reproduces successfully the PE dynamics; compare left panel of Fig. 14 with the lower-left panel of Fig. 7 and the center panel of Fig. 13. For $\epsilon = 1.5518$ falling within Regime III (the fuzzy-manifold regime), the QG manifold fails dramatically in filtering out the fast, small-amplitude oscillations contained in the PE solutions; compare with the lower-left panel of Fig. 8. For that ϵ-value as well as for any others, the (x_1, x_2)-projection is to the best a vertical segment when the tangent manifold Ψ is used instead of the BE manifold. The latter property results from the definition of Ψ in (4.17).

Finally drastic failures are shown in Figs. 13 and 14 for $\epsilon = \epsilon_*$, when either the QG or the tangent manifold is used; compare with the lower-left panel of Fig. 9.

[15] Actually we numerically observed, given the ϵ-resolution used in our experiments, that the QG dynamics settles down to a steady state for $\epsilon \leq 1.01167487$.

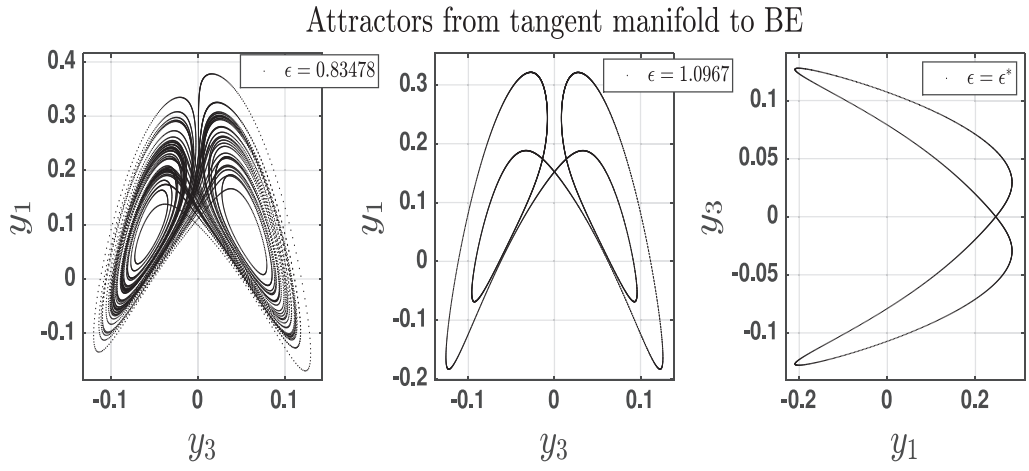

Fig. 13. Attractors associated with Eq. (3.10) in which the tangent manifold Ψ replaces the BE manifold Φ.

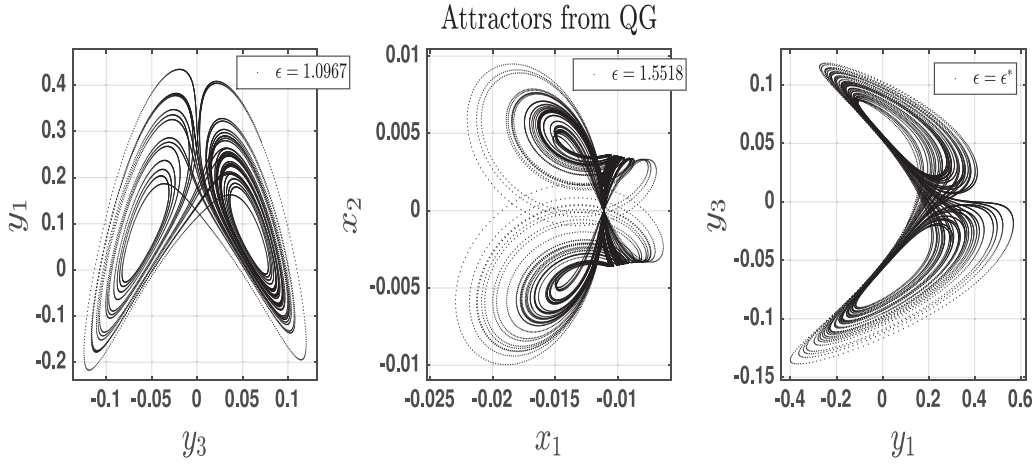

Fig. 14. Attractors associated with QG model (2.6).

This comparison across few ϵ-values reveals the unsatisfactory behavior of the modeling skills when either the tangent manifold to BE or the QG manifold is used. This is in sharp contrast with the good modeling skills of the BE manifold discussed earlier for $\epsilon < \epsilon_*$, and further supports the idea that even a small fraction of energy of the fast variables requires an appropriate parameterization and that the BE manifold seems to provide such a parameterization. We turn now to a final but important discussion about the case $\epsilon \geq \epsilon_*$.

4.3. Non-Markovian stochastic corrections to the slow conditional expectation

Thus, it can be reasonably conjectured that the BE manifold is close to the optimal PM for $\epsilon < \epsilon_*$ and that for $\epsilon \geq \epsilon_*$, the minimum of the parameterizing defect functional (4.8) (when normalized by the mean energy contained $\mathbf{x}$) is expected to be, in general, rather close to 1 (from below) than to zero for ϵ-values corresponding to Regime IV of explosive fast oscillations.

This feature manifested in the parameterization defect Q (see Fig. 12), strongly indicates that a nonlinear parameterization of slaving-type is insufficient when $\epsilon \geq \epsilon_*$ for which the fraction of energy contained in the fast variable $\mathbf{x}$ becomes substantial in the course of time (see Fig. 5 again) due to the presence of the explosive bursts.

At the same time and as mentioned above, Figs. 9 and 10 strongly suggest that even for $\epsilon \geq \epsilon_*$ the BE manifold may be regarded as providing a good approximation of the optimal PM in the sense that the latter, from its definition (4.6), is expected to average out the fast oscillations which also does the BE manifold in those cases, although only partially in other instances such as shown in Fig. 11.

Comforted therefore by the idea that the BE provides a good approximation of the slow conditional expectation, we are thus left with the analysis of the corrective terms to be added to the BE, for $\epsilon \geq \epsilon_*$. The Mori–Zwanzig (MZ) formalism [8,71] as formulated within the framework of forced-dissipative chaotic systems [66, 67, 33, Section 4], allows us to predict the nature of these corrective terms. More exactly, it can be proved that the optimal reduced model describing the evolution of the slow variables takes the following form:

$$\dot{\mathbf{y}} = \overline{\Pi_s \mathbf{R}}(\mathbf{y}) + \int_0^t \mathbf{G}(t, s, \mathbf{y}(s))\, \mathrm{d}s + \eta_t, \qquad \text{(GLE)}$$

known as the *generalized Langevin equation (GLE).*

Here, the nonlinear vector field, $\overline{\Pi_s \mathbf{R}}$ given in (4.7), represents the *Markovian contribution* that accounts for the nonlinear self-interactions among the slow variables and some cross-interactions with the fast variables as parameterized by the optimal PM h defined in (4.6). The integral term accounts for the cross-interactions between the slow and fast variables not accounted by h; it involves the past of the slow variables and conveys *non-Markovian*

(i.e. memory) effects[16] and arises from the fluctuations of the projected vector field $\Pi_{\mathfrak{s}}\mathbf{R}$, with respect to slow conditional expectation $\overline{\Pi_{\mathfrak{s}}\mathbf{R}}$ [33, Sec. 4] i.e. here from the terms $B_2\big(\mathbf{y}, \mathbf{x}-h(\mathbf{y})\big)$ and $\mathbf{x}-h(\mathbf{y})$, by using (4.7). Finally, the η_t-term accounts for effects of the fast variables which are uncorrelated with the slow variables. This last term can be thus represented by a *state-independent noise* that may still involve correlations in time, e.g. of "red noise" type[17].

It is worth noticing that different approaches based on matched asymptotic expansions of flows have pointed out the usefulness of integral terms involving time-history of the slow variables to rectify the slow manifold picture [22]. In the context of shallow-water equations in the small-Froude-number limit $\mathbf{F} \ll 1$, with a Rossby number $\epsilon = \mathcal{O}(1)$, the authors of [22] showed indeed that terms involving time-history of the potential vorticity and emerging at order $O(\mathbf{F}^4)$, may be used to measure the degree of "fuzziness," i.e. to take into account the effects on the flow of the aforementioned fluctuating terms.

From a general viewpoint, the analytical determination of the constitutive elements of the GLE is a difficult task in practice, and only problem-specific analytic solutions have been proposed in the literature [7,29,54]; see also [10,33] for a data-driven approach to this problem. In the context of this article, given the ability of the BE manifold to be indistinguishable from the slow/fuzzy manifold (with a small parameterization defect Q) or to average out the fast oscillations (even for (some) $\epsilon \geq \epsilon_*$ when Q gets close to 1), one can reasonably infer that the BE manifold provides a good analytic approximation[18] of the slow conditional expectation $\overline{\Pi_{\mathfrak{s}}\mathbf{R}}$ given in (4.7) by the following (slow) vector field of $\mathscr{H}_{\mathfrak{s}}$, i.e.:

$$\mathbf{R}_{\mathrm{BE}} \approx \overline{\Pi_{\mathfrak{s}}\mathbf{R}}, \quad \text{with} \quad \mathbf{R}_{\mathrm{BE}} : \mathbf{y} \mapsto L\mathbf{y} + B_1\big(\mathbf{y}, \mathbf{y}\big) + B_2\big(\mathbf{y}, \Phi(\mathbf{y})\big) - \Phi(\mathbf{y}), \tag{4.24}$$

where Φ is given in (3.9) (up to the rescaling (3.11)).

We have observed (not shown) that the rectification of the BE manifold in situations of partial failure of averaging, such as reported in Fig. 11, can be made possible by adapting the backward-forward approach of [9,12] to build PMs associated with Eq. (2.5) even closer to the optimal PM than the BE manifold is. These refined but important rectifications to BE will be communicated elsewhere. However, such corrections lie still at the level of the conditional expectation, i.e. in efforts for improving the approximation in (4.24). An efficient analytic determination of the memory and noise terms that would allow thus for a recovering of the high-frequency variability of the PE solutions after the emergence of explosive fast oscillations, remain still an open question.

5. Discussion

Thus, the perspective on the slow manifold (and its implications for forecast initialization) from the 9D PE model differs from the exponentially small "fuzziness" $\epsilon \to 0$ perspective motivated by the simplified 5D model [38,60]: our extensive numerical study strongly suggests indeed that a slow manifold does exist for a finite range of Rossby numbers, it becomes "fuzzy" due to weak fast oscillations at higher Rossby numbers, and it fails catastrophically to exist at a critical Rossby number ϵ_* with an explosion of energetic fast oscillations.

In that respect, a novel variational perspective on the closure problem exploiting manifolds has been introduced. This framework allows for a unification of previous concepts such as the slow manifold or other concepts of "fuzzy" manifold. It allows furthermore for a rigorous identification of an optimal limiting object for the averaging of fast oscillations, namely the optimal parameterizing manifold (PM). We have shown that the manifold underlying the nonlinear Balance Equations provides a very good approximation of this optimal PM even somewhat beyond the emergence of fast and energetic oscillations.

The nonlinear Balance Equations (BE) are therefore a successful slow-manifold parameterizing model up to the limit of PE slowness and even fuzzy slowness, and it even has some skill for the slow components beyond this point; each of these properties showing together that the BE constitutes a good approximation of the slow conditional expectation; see (4.24). Still, a more complete closure theory is needed that also encompasses the fast oscillations beyond the critical dynamical transition occurring at ϵ_*, including non-Markovian and stochastic effects as discussed in Section 4.3.

The parameterizing manifold approach provides thus a new framework to understand how such reduced models relate to full PE solutions although open questions remain beyond ϵ_*. There is growing evidence from turbulent simulations that balance and slowness generically fail at finite Rossby number [18,44,46,47,49,69], although further dynamical clarification is needed for how this occurs. In particular, the existence of a critical ϵ_* such as exhibited above remains still to be analyzed for the full set of PDEs associated with a PE formulation. Although individual triad interactions of slow-fast variables may exhibit similar critical behavior, their collective coupled dynamics for higher dimensional truncation may lead to less brutal dynamical transitions than reported here. Whether or not large-scale flows are truly slow or merely asymptotically so, a "proper (slow) balance" initialization remains an essential ingredient for forecasts with the PE.

Acknowledgments

This work has been partially supported by the Office of Naval Research (ONR) Multidisciplinary University Research Initiative (MURI) grant N00014-12-1-0911 and N00014-16-1-2073 (MDC). We thank one of the anonymous reviewers. His/her inspiring and constructive remarks were greatly appreciated.

Appendix A. The optimal parameterizing manifold

Given the invariant measure μ of the rescaled PE that satisfies the ergodic property (4.3), one denotes hereafter by $\mathfrak{m}$ the probability measure obtained as push-forward of μ onto the slow vector space $\mathscr{H}_{\mathfrak{s}}$ and by ν, that obtained as push-forward of μ onto the slow-fast vector space $\mathscr{H}_{\mathfrak{f}_1} \times \mathscr{H}_{\mathfrak{s}}$. Hereafter we drop again the ϵ-subscript to avoid superfluous notations.

One denotes finally by $\mathscr{F}_{\mathfrak{s}}$ the Hilbert space constituted by $\mathscr{H}_{\mathfrak{f}_1}$-valued functions (of the slow variables) that are square-integrable with respect to $\mathfrak{m}$ i.e.,

$$\mathscr{F}_{\mathfrak{s}} = L^2_{\mathfrak{m}}(\mathscr{H}_{\mathfrak{s}}; \mathscr{H}_{\mathfrak{f}_1}) = \Big\{ \Psi : \mathscr{H}_{\mathfrak{s}} \to \mathscr{H}_{f_1} \text{ measurable and such that } \times \int_{\mathscr{H}_{\mathfrak{s}}} \|\Psi(\mathbf{y})\|^2 \, \mathrm{d}\mathfrak{m}(\mathbf{y}) < \infty \Big\}. \tag{A.1}$$

Theorem A.1. *The optimal manifold that averages out the fast variables* $\mathbf{x}$ *in* $\mathscr{H}_{f_1}$, *is given as the graph of*

$$h(\mathbf{y}) = \int_{\mathscr{H}_{\mathfrak{s}}} \mathbf{x} \, \mathrm{d}\mu^1_{\mathbf{y}}(\mathbf{x}), \tag{A.2}$$

[16] The non-Markovian effects considered here are endogenous, i.e. depend on the past of the solution itself. These effects are different from those discussed in [12] which arise in the reduction of stochastic systems, and are exogenous, i.e. depending on the past of the noise.

[17] We refer to e.g. [26,31,34,50] for similar but different stochastic replacement of (chaotic) fast variables in related systems.

[18] Up to the inversion of the matrix M with nonlinear entries in (3.9).

where $\mu^1_{\mathbf{y}}$ denotes the disintegrated probability distribution on the vector space $\mathscr{H}_{\mathfrak{f}_1}$ of the fast variable $\mathbf{x}$*, and that is conditioned on the slow variable* $\mathbf{y}$*; see (4.5).*

This manifold is optimal in the sense that h given in (A.2) minimizes

$$J(\Psi) = \lim_{T\to\infty} \frac{1}{T}\int_0^T \left\|\mathbf{x}(t) - \Psi(\mathbf{y}(t))\right\|^2 \mathrm{d}t, \quad (\mathbf{x}(t), \mathbf{y}(t), \mathbf{z}(t)) \in \mathscr{A},\ \Psi \in \mathscr{F}_{\mathfrak{s}}. \tag{A.3}$$

If furthermore $J(h) < \lim_{T\to\infty} \frac{1}{T}\int_0^T \|\mathbf{x}(t)\|^2 \mathrm{d}t$, then h is the optimal parameterizing manifold.[19]

Proof. Let us introduce the following Hilbert space of $\mathscr{H}_{\mathfrak{f}_1}$-valued functions of the slow-fast variables

$$L^2_\nu(\mathscr{H}_{\mathfrak{f}_1}\times\mathscr{H}_{\mathfrak{s}};\mathscr{H}_{\mathfrak{f}_1}) : = \left\{ f : \mathscr{H}_{\mathfrak{f}_1}\times\mathscr{H}_{\mathfrak{s}} \to \mathscr{H}_{\mathfrak{f}_1},\ \text{measurable and such that} \times \int_{\mathscr{H}_{\mathfrak{f}_1}\times\mathscr{H}_{\mathfrak{s}}} \|f(\mathbf{x},\mathbf{y})\|^2 \mathrm{d}\nu(\mathbf{x},\mathbf{y}) < \infty \right\}. \tag{A.4}$$

Because ν is a probability measure, any function Ψ in $\mathscr{F}_{\mathfrak{s}}$ can be embedded[20] as a function that lives in $L^2_\nu(\mathscr{H}_{\mathfrak{f}_1}\times\mathscr{H}_{\mathfrak{s}};\mathscr{H}_{\mathfrak{f}_1})$.

With this functional setting, one can thus apply, in the ambient Hilbert space $L^2_\nu(\mathscr{H}_{\mathfrak{f}_1}\times\mathscr{H}_{\mathfrak{s}};\mathscr{H}_{\mathfrak{f}_1})$, the standard projection theorem onto closed convex sets [2, Theorem 5.2] to define (given $\Pi_{\mathfrak{s}}$) the slow conditional expectation $\mathbb{E}[g|\Pi_{\mathfrak{s}}]$ of g as the unique function in $\mathscr{F}_{\mathfrak{s}}$ that satisfies the inequality

$$\mathbb{E}[\|g - \mathbb{E}[g|\Pi_{\mathfrak{s}}]\|^2] \le \mathbb{E}[\|g-\Psi\|^2],\ \text{for all } \Psi\in\mathscr{F}_{\mathfrak{s}}, \tag{A.5}$$

where the expectation $\mathbb{E}(g)$ is taken with respect to probability measure ν, that is:

$$\mathbb{E}(g) = \int_{\mathscr{H}_{\mathfrak{f}_1}\times\mathscr{H}_{\mathfrak{s}}} g(\mathbf{x},\mathbf{y})\,\mathrm{d}\nu(\mathbf{x},\mathbf{y}). \tag{A.6}$$

The general disintegration theorem of probability measures [16, p. 78], applied to ν (see (4.5)),[21] allows us then to have the following explicit representation of the slow conditional expectation

$$\mathbb{E}[g|\Pi_{\mathfrak{s}}] = \int_{\mathscr{H}_{\mathfrak{s}}} g(\mathbf{x},\mathbf{y})\,\mathrm{d}\mu^1_{\mathbf{y}}(\mathbf{x}). \tag{A.7}$$

Here $\mu^1_{\mathbf{y}}$ denotes the disintegrated probability distribution on the fast vector space $\mathscr{H}_{\mathfrak{f}_1}$ and that is conditioned on the slow variable $\mathbf{y}$; see (4.5) and [13, Supporting Information].

Now let us take $g = \xi$ with $\xi(\mathbf{x},\mathbf{y}) = \mathbf{x}$, then from (A.5), we deduce

$$\mathbb{E}[\|\xi - h\|^2] \le \mathbb{E}[\|\xi-\Psi\|^2],\quad \text{for all } \Psi\in\mathscr{F}_{\mathfrak{s}}, \tag{A.8}$$

with h given by (A.2).

By noting that

$$\mathbb{E}[\|\xi - h\|^2] = \int_{\mathscr{H}_{\mathfrak{f}_1}\times\mathscr{H}_{\mathfrak{s}}} \|\mathbf{x} - h(\mathbf{y})\|^2\,\mathrm{d}\nu(\mathbf{x},\mathbf{y}) = \int_{\mathscr{H}} \|x - h(\mathbf{y})\|^2\,\mathrm{d}\mu(\mathbf{x},\mathbf{y},\mathbf{z}), \tag{A.9}$$

(and similarly for Ψ) one obtains then, by applying respectively (4.3) to $\varphi = \|\xi - h\|^2$ and $\varphi = \|\xi-\Psi\|^2$, that

$$\lim_{T\to\infty}\frac{1}{T}\int \|\mathbf{x}(t) - h(\mathbf{y}(t))\|^2\,\mathrm{d}t \le \lim_{T\to\infty}\frac{1}{T}\int \|\mathbf{x}(t) - \Psi(\mathbf{y}(t))\|^2\,\mathrm{d}t, \tag{A.10}$$

for all Ψ in $\mathscr{F}_{\mathfrak{s}}$. The proof is complete. □

Remark A.1.

(i) The above theorem is not limited to the rescaled PE system and could apply to any relevant Fourier truncation of the PE system of partial differential equations (PDEs) considered in [40].

(ii) The ergodic property (4.3) can be relaxed in to weaker forms such as in e.g. [6,23] that hold for a broad class of dissipative systems including systems of PDEs, as long as a global attractor exists [6, Theorem 2.2]. In the infinite-dimensional setting of PDEs, the uniqueness of the statistical equilibrium μ that satisfies such a weak form of ergodicity is not guaranteed and the limit in (A.3) have to be replaced by generalized versions involving e.g. averaging over accumulations points. With these changes in mind, the proof presented above can be easily adapted and the conclusion of Theorem A.1 remains valid with however a form of optimality that is now subject to the choice of the statistical equilibrium. Within this framework, several optimal parameterizing manifolds may co-exist but for each statistical equilibrium there is only one optimal parameterizing manifold.

[19] Note that we always have $J(h) \le \lim_{T\to\infty}\frac{1}{T}\int_0^T \|\mathbf{x}(t)\|^2\,\mathrm{d}t = J(0)$, given that h minimizes J.

[20] By simply setting $\tilde{\Psi}(\mathbf{x},\mathbf{y}) := \Psi(\mathbf{y})$ for all $\mathbf{x}$.

[21] The disintegration formula is written in (4.5) for the probability measure μ, but since $\int_{\mathscr{H}} g(\mathbf{x},\mathbf{y})\,\mathrm{d}\mu = \int_{\mathscr{H}_{\mathfrak{f}_1}\times\mathscr{H}_{\mathfrak{s}}} g(\mathbf{x},\mathbf{y})\,\mathrm{d}\nu$, the formula could be equivalently applied to ν. We still denote by $\mu^1_{\mathbf{y}}$ the associated disintegrated measure to relate it to the statistical equilibrium μ.

References

[1] Arnold VI. Geometrical methods in the theory of ordinary differential equations. second. Springer-Verlag, New York; 1988.
[2] Brézis H. Functional analysis, sobolev spaces and partial differential equations. Springer; 2010.
[3] Baer F, Tribbia JJ. On complete filtering of gravity modes through nonlinear initialization. Month Weather Rev 1977;105(12):1536–9.
[4] Camassa R. On the geometry of an atmospheric slow manifold. Physica D 1995;84(3):357–97.
[5] Collet P, Eckmann J-P. Concepts and results in chaotic dynamics: a short course. Springer; 2007.
[6] Chekroun MD, Glatt-Holtz NE. Invariant measures for dissipative dynamical systems: abstract results and applications. Commun Math Phys 2012;316(3):723–61.
[7] Chorin AJ, Hald OH. Stochastic tools in mathematics and science. Surveys and Tutorials in the Applied Mathematical Sciences. Springer New York; 2006. no. 147
[8] Chorin AJ, Hald OH, Kupferman R. Optimal prediction with memory. Physica D 2002;166(3):239–57.
[9] Chekroun MD, Liu H. Finite-horizon parameterizing manifolds, and applications to suboptimal control of nonlinear parabolic PDEs. Acta Applicandae Mathematicae 2015;135(1):81–144.
[10] Chorin AJ, Lu F. Discrete approach to stochastic parametrization and dimension reduction in nonlinear dynamics. Proc Natl Acad Sci USA 2015;112(32):9804–9.
[11] Chekroun MD, Liu H, Wang S. Approximation of stochastic invariant manifolds: stochastic manifolds for nonlinear SPDEs I. New York: Springer Briefs in Mathematics, Springer; 2015b.
[12] Chekroun MD, Liu H, Wang S. Stochastic parameterizing manifolds and non–Markovian reduced equations: stochastic manifolds for nonlinear SPDEs II. New York: Springer Briefs in Mathematics, Springer; 2015a.
[13] Chekroun MD, Neelin JD, Kondrashov D, McWilliams JC, Ghil M. Rough parameter dependence in climate models: The role of Ruelle-Pollicott resonances. Proc Natl Acad Sci USA 2014;111(5):1684–90.
[14] Chekroun MD, Simonnet E, Ghil M. Stochastic climate dynamics: random attractors and time-dependent invariant measures. Physica D 2011;240(21):1685–700.
[15] Camassa R, Tin S-K. The global geometry of the slow manifold in the lorenz-krishnamurthy model. J Atmos Sci 1996;53(22):3251–64.
[16] Dellacherie C, Meyer P-A. Probabilities and potential, north-Holland mathematics studies, vol.29. North-Holland Publishing Co.; 1978.
[17] Debussche A, Temam R. Inertial manifolds and the slow manifolds in meteorology. Differ Integral Eq 1991;4(5):897–931.
[18] Deusebio E, Vallgren A, Lindborg E. The route to dissipation in strongly stratified and rotating flows. J Fluid Mech 2013;720:66–103.

[19] Eckmann J-P, Ruelle D. Ergodic theory of chaos and strange attractors. Rev Modern Phys 1985;57:617–56.
[20] Fenichel N. Persistence and smoothness of invariant manifolds for flows. Indiana Univ Math J 1972;21(3):193–226.
[21] Fenichel N. Geometric singular perturbation theory for ordinary differential equations. J Differ Eq 1979;31(1):53–98.
[22] Ford R, McIntyre ME, Norton WA. Balance and the slow quasimanifold: some explicit results. J Atmos Sci 2000;57(9):1236–54.
[23] Foias C, Manley O, Rosa R, Temam R. Navier-Stokes equations and turbulence. Encyclopedia of Mathematics and its Applications, vol.83. Cambridge: Cambridge University Press; 2001. ISBN 0-521-36032-3
[24] Foias C, Manley O, Temam R. Modelling of the interaction of small and large eddies in two-dimensional turbulent flows. RAIRO Modél Math Anal Numér 1988;22(1):93–118.
[25] Gallavotti G, Cohen EGD. Dynamical ensembles in stationary states. J Stat Phys 1995;80(5–6):931–70.
[26] Givon D, Kupferman R, Stuart A. Extracting macroscopic dynamics: model problems and algorithms. Nonlinearity 2004;17(6):R55–R127.
[27] Gent PR, McWilliams JC. Intermediate model solutions to the Lorenz equations: Strange attractors and other phenomena. J Atmos Sci 1982;39(1):3–13.
[28] Holm DD. Hamiltonian balance equations. Physica D 1996;98(2):379–414.
[29] Hald OH, Stinis P. Optimal prediction and the rate of decay for solutions of the euler equations in two and three dimensions. Proc Natl Acad Sci USA 2007;104(16):6527–32.
[30] Jacobs SJ. Existence of a slow manifold in a model system of equations. J AtmosSci 1991;48(7):893–902.
[31] Just W, Kantz H, Rödenbeck Ch, Helm M. Stochastic modelling: replacing fast degrees of freedom by noise. J Phys A 2001;34(15):3199–213.
[32] Jones CKRT. Geometric singular perturbation theory. In: Dynamical systems. Springer; 1995. p. 44–118.
[33] Kondrashov D, Chekroun MD, Ghil M. Data-driven non-Markovian closure models. Physica D 2015;297:33–55. doi:10.1016/j.physd.2014.12.005.
[34] Kantz H, Just W, Baba N, Gelfert K, Riegert A. Fast chaos versus white noise: entropy analysis and a Fokker-Planck model for the slow dynamics. Physica D 2004;187(1):200–13.
[35] Kopell N. Invariant manifolds and the initialization problem for some atmospheric equations. Physica D 1985;14(2):203–15.
[36] Lang S. Real and functional analysis, 3rd Edition, vol. 142. Graduate Texts in Mathematics, Springer; 1993.
[37] Leith CE. Nonlinear normal mode initialization and quasi-geostrophic theory. J Atmos Sci 1980;37(5):958–68.
[38] Lorenz EN, Krishnamurthy V. On the nonexistence of a slow manifold. J Atmos Sci 1987;44(20):2940–50.
[39] Lorenz EN. Deterministic nonperiodic flow. J Atmos Sci 1963;20(2):130–41.
[40] Lorenz EN. Attractor sets and quasi-geostrophic equilibrium. J Atmos Sci 1980;37(8):1685–99.
[41] Lorenz EN. On the existence of a slow manifold. J Atmos Sci 1986;43(15):1547–58.
[42] Lorenz EN. The slow manifold-what is it? Journal of the atmospheric sciences 1992;49(24):2449–51.
[43] Machenhauer B. On the dynamics of gravity oscillations in a shallow water model with applications to normal mode initialization. Beitr Phys Atmos 1977;50:253–71.
[44] McWilliams JC. Submesoscale Currents in the Ocean. Proc R Soc A 2016. In press.
[45] McWilliams JC, Gent PR. Intermediate models of planetary circulations in the atmosphere and ocean. J Atmos Sci 1980;37(8):1657–78.
[46] Molemaker MJ, McWilliams JC, Capet X. Balanced and unbalanced routes to dissipation in an equilibrated eady flow. J Fluid Mech 2010;654:35–63.
[47] Marino R, Pouquet A, Rosenberg D. Resolving the paradox of oceanic large-scale balance and small-scale mixing. Phys RevLett 2015;114(11):114504.
[48] McWilliams JC, Yavneh I, Cullen MJP, Gent PR. The breakdown of large-scale flows in rotating, stratified fluids. Phys Fluids (1994-present) 1998;10(12):3178–84.
[49] Nadiga BT. Nonlinear evolution of a baroclinic wave and imbalanced dissipation. J Fluid Mech 2014;756:965–1006.
[50] Papanicolaou GC. Some probabilistic problems and methods in singular perturbations. J Math 1976;6(4):653–74.
[51] Plougonven R, Zhang F. Internal gravity waves from atmospheric jets and fronts. Rev Geophys 2014;52(1):33–76.
[52] Roques L, Chekroun MD. Probing chaos and biodiversity in a simple competition model. Ecol Complexity 2011;8(1):98–104.
[53] Rosa R. Approximate inertial manifolds of exponential order. Dyn Syst 1995;1(3):421–48.
[54] Stinis P. Higher-order Mori-Zwanzig models for the Euler equations. Multis Model Simul 2007;6(3):741–60.
[55] Temam R. Infinite-dimensional dynamical systems in mechanics and physics, vol.68. Springer Science & Business Media; 2012.
[56] Tikhonov AN. Systems of differential equations containing small parameters in the derivatives. Matematicheskii sbornik 1952;73(3):575–86.
[57] Temam R, Wirosoetisno D. Stability of the slow manifold in the primitive equations. SIAM J Math Anal 2010;42(1):427–58.
[58] Temam R, Wirosoetisno D. Slow manifolds and invariant sets of the primitive equations. J Atmos Sci 2011;68(3):675–82.
[59] Vanneste J. Inertia-gravity wave generation by balanced motion: revisiting the lorenz-krishnamurthy model. J Atmos Sci 2004;61(2):224–34.
[60] Vanneste J. Balance and spontaneous wave generation in geophysical flows. Ann Rev Fluid Mech 2013;45:147–72.
[61] Viúdez A, Dritschel DG. Spontaneous generation of inertia–gravity wave packets by balanced geophysical flows. J Fluid Mech 2006;553:107–17.
[62] Vautard R, Legras B. Invariant manifolds, quasi-geostrophy and initialization. J Atmos Sci 1986;43(6):565–84.
[63] Vanneste J, Yavneh I. Exponentially small inertia-gravity waves and the breakdown of quasigeostrophic balance. J Atmos Sci 2004;61(2):211–23.
[64] Vanneste J, Yavneh I. Unbalanced instabilities of rapidly rotating stratified shear flows. J Fluid Mech 2007;584:373–96.
[65] Warn T. Nonlinear balance and quasi-geostrophic sets. Atmosphere-Ocean 1997;35(2):135–45.
[66] Wouters J, Lucarini V. Disentangling multi-level systems: averaging, correlations and memory. J Stat Mech 2012(3):P03003.
[67] Wouters J, Lucarini V. Multi-level dynamical systems: connecting the Ruelle response theory and the Mori-Zwanzig approach. J Stat Phys 2013;151(5):850–60.
[68] Warn T, Menard R. Nonlinear balance and gravity-inertial wave saturation in a simple atmospheric model. Tellus A 1986;38(4):285–94.
[69] Yavneh I, Mcwilliams JC. Breakdown of the slow manifold in the shallow-water equations. Geophys Astrophys Fluid Dyn 1994;75(2–4):131–61.
[70] Young L-S. What are SRB measures, and which dynamical systems have them? J Stat Phys 2002;108(5):733–54.
[71] Zwanzig R. Nonequilibrium statistical mechanics. Oxford University Press; 2001.

Please cite this article as: M.D. Chekroun et al., The emergence of fast oscillations in a reduced primitive equation model and its implications for closure theories, Computers and Fluids (2016), http://dx.doi.org/10.1016/j.compfluid.2016.07.005